Lithos 314–315 (2018) 140–155

Contents lists available at ScienceDirect

Lithos

journal homepage: www.elsevier.com/locate/lithos

Detrital apatite U-Pb and trace element analysis as a provenance tool: Insights from the Yenisey Ridge (Siberia)

J. Gillespie [a,*], S. Glorie [a], A. Khudoley [b], A.S. Collins [a]

[a] Centre for Tectonics, Resources, and Exploration (TRaX), Department of Earth Sciences, The University of Adelaide, 5005, Australia
[b] Institute of the Earth Sciences, St. Petersburg State University, 7/9 University Embankment, St. Petersburg 199034, Russia

ARTICLE INFO

Article history:
Received 6 March 2018
Accepted 23 May 2018
Available online 26 May 2018

Keywords:
Apatite
Provenance
Detrital
U-Pb
LA-ICP-MS
Rare earth elements

ABSTRACT

The use of zircon U-Pb geochronology to study the provenance of sediment is well-established, yet there are fundamental biases that are hard to avoid. These biases are due, in part, to the limited range of magmatic compositions from which zircon will crystallise. This can manifest as the over/under representation of particular age populations (i.e. sediment sources) in the data. The analysis of apatite, a mineral found in a wide variety of igneous rocks, can help to address this bias in detrital geochronology. In this study, we combine geochemical and U-Pb LA-ICP-MS analysis of individual apatite grains to characterise the potential source rocks. This information is integrated with zircon U-Pb data from the same samples in order to demonstrate the complementary provenance information that can be derived from apatite and zircon archives. The analysis of detrital apatite from sedimentary rocks in the Yenisey Ridge (Siberia) found two main U-Pb age populations. An apatite U-Pb population at 880–720 Ma corresponds to Neoproterozoic magmatism in the Yenisey Ridge, and a second at ~1800 Ma to magmatism related to the assembly of the Siberian Craton. Abundant Neoproterozoic apatites, many of which have chemistries indicative of crystallising from a mafic magma, are considerably more common than the relatively rare zircons of the same age. The ability of apatite analysis to detect mafic magmatic sources is one of the strengths of this approach that makes it particularly useful when used in combination with zircon U-Pb geochronology. This study shows that multi-method analysis of detrital apatite has the potential to be an important tool in conjunction with detrital zircon analysis in future efforts to understand the provenance of sedimentary rocks.

1. Introduction

Sedimentary basins provide an archive of the tectonic history of their surroundings, making them an invaluable source of information for palaeogeographic and palaeotectonic studies. Studies concerning sedimentary provenance frequently rely on the distribution of zircon U-Pb ages and Hf isotopic composition to understand the sources of sediment, drawing conclusions about the geological history of the basin by comparing detrital age distributions to those found in other basins or in potential source regions (e.g. Bruguier et al., 1997; Cawood et al., 2003; Dickinson and Gehrels, 2003; LaMaskin, 2012; Schoene, 2014). Advances in the statistical methods for displaying and understanding zircon U-Pb data (e.g. KDE and MDS plots; Vermeesch (2012, 2013)) have improved our ability to effectively interpret and communicate these results (e.g. Armistead et al., 2018; Yang et al., 2018).

However, fundamental sources of biases in the detrital zircon record remain, such as the limited range of magmatic compositions that readily produce zircon and the high preservation potential of this mineral (e.g. Andersen et al., 2016; Malusà et al., 2016; Spencer et al., 2018). The zircon fertility of rocks with similar lithologies can differ by as much as half an order of magnitude (Dickinson, 2008; Moecher and Samson, 2006), while different source regions in the European Alps were found to vary in zircon fertility by five orders of magnitude (Malusà et al., 2016). The typically low zircon fertility of mafic rocks means that sources dominantly composed of mafic rocks are at risk of being under-represented or rendered invisible in the detrital zircon record (Moecher and Samson, 2006). The consequence of these limitations is that detrital zircon age distributions usually do not accurately reflect the proportional contribution of source rocks to the sediment.

In contrast to zircon, apatite grows in both felsic and mafic rocks (Piccoli and Candela, 2002). Furthermore, because the trace element and rare earth element (REE) chemistry of magmatic apatite is sensitive to the composition of the host rock, the analysis of these elements via LA-ICP-MS can be used to understand the source of detrital apatite grains (e.g. Belousova et al., 2002; Morton and Yaxley, 2007). The ability to geochemically characterise detrital apatites as being mafic in origin (Belousova et al., 2002; Bruand et al., 2017; Jennings et al., 2011; Morton and Yaxley, 2007) is important, because this means that apatite analysis can be used to help address fundamental issues in relation to

* Corresponding author.
E-mail address: jack.gillespie@adelaide.edu.au (J. Gillespie).

https://doi.org/10.1016/j.lithos.2018.05.026
0024-4937/

biases in the detrital record. As apatite is more susceptible to chemical and physical weathering than zircon (Morton and Hallsworth, 1999), detrital apatite is more likely to be representative of first-cycle sediment, but also faces an increased risk of destruction between the time of formation and the present. Apatite is very stable during burial and diagenesis but is less stable under some weathering conditions, such as during acidic soil formation, where it is relatively easily dissolved (Morton and Hallsworth, 1999). U-Pb dating of apatite is complicated by typically low U concentrations and the variable incorporation of non-radiogenic (common) Pb, although the development of new standards and data reduction protocol specifically for apatite U-Pb dating has helped address this problem (e.g. Chew et al., 2014b; Thomson et al., 2012).

Although some published studies have applied detrital apatite geochemistry (Abdullin et al., 2016; Jafarzadeh et al., 2014; Morton and Yaxley, 2007), or U-Pb geochronology (Carrapa et al., 2009; Mark et al., 2016; Painter et al., 2014; Zattin et al., 2012) as a provenance tool, this study presents the novel combination of U-Pb and trace element LA-ICP-MS analysis on individual apatite grains to investigate the provenance of ancient sedimentary rocks. We apply this approach to investigate the provenance of sedimentary and metasedimentary rocks from the Yenisey Ridge, Russia. This case study demonstrates that the combination of multi-method apatite and zircon U-Pb analyses mitigates the drawbacks of either approach in isolation, and illustrates how these methods provide complementary and intersecting information about the provenance of the original sediment.

2. Geological setting

2.1. Study area: Yenisey Ridge

The Yenisey Ridge is a fold and thrust belt stretching >700 km NW–SE along the western margin of the Siberian Craton (Fig. 1; Likhanov and Santosh, 2017). This contentious and poorly understood area is important for understanding the palaeogeography of Siberia during the Neoproterozoic and Mesoproterozoic, as different tectonic models have implications for the position of Siberia with relation to other continents in the supercontinent Rodinia (Kuzmichev and Sklyarov, 2016; Likhanov et al., 2015; Merdith et al., 2017; Vernikovsky et al., 2016).

The ENE striking strike-slip Angara Fault divides the Yenisey Ridge into two regions. The northern region (Transangaria) comprises the Isakov, Central Angara, and East Angara terranes, while the southern region is composed of the Angara-Kan and Predivinsk terranes (Fig. 1; Kuzmichev and Sklyarov, 2016). To the north of the Angara fault, Transangaria is composed primarily of Meso-Neoproterozoic rock, while the southern region includes both the Palaeoproterozoic Angara-Kan and the Neoproterozoic Predivinsk terranes (Vernikovsky et al., 2016). Most of the major structures in the belt strike NW, including the Ishimba thrust that separates the East and Central Angara terranes (Kuzmichev and Sklyarov, 2016).

Both the Central Angara and East Angara terranes are characterised by variably metamorphosed rocks reaching amphibolite facies in the Central Angara terrane and decreasing eastward (Mel'nikov et al., 2005). The East Angara terrane experienced no Neoproterozoic magmatism, while in contrast the Central Angara terrane was intruded by several phases of Tonian magmatism (880–720 Ma) (Vernikovsky et al., 2003; Vernikovsky et al., 2016). The Isakov terrane is mostly composed of volcanogenic-sedimentary and ophiolitic units that are thought to be the remains of an island arc thrust onto the western margin of the Central Angara terrane at ~630 Ma (Vernikovsky et al., 2003).

The East Angara terrane contains rocks of the deformed passive margin of the Siberian Craton, dating to the Meso- and Neoproterozoic (Nozhkin et al., 2009; Vernikovsky et al., 2003; Vernikovsky et al., 2016). The main topic of discussion in the published literature concerning the tectonic evolution of the Yenisey Ridge is the origin and position of the Central Angara terrane (Vernikovsky et al., 2003; Vernikovsky et al., 2016). Vernikovsky et al. (2016) consider the Central Angara terrane to have been an independent block until it collided with

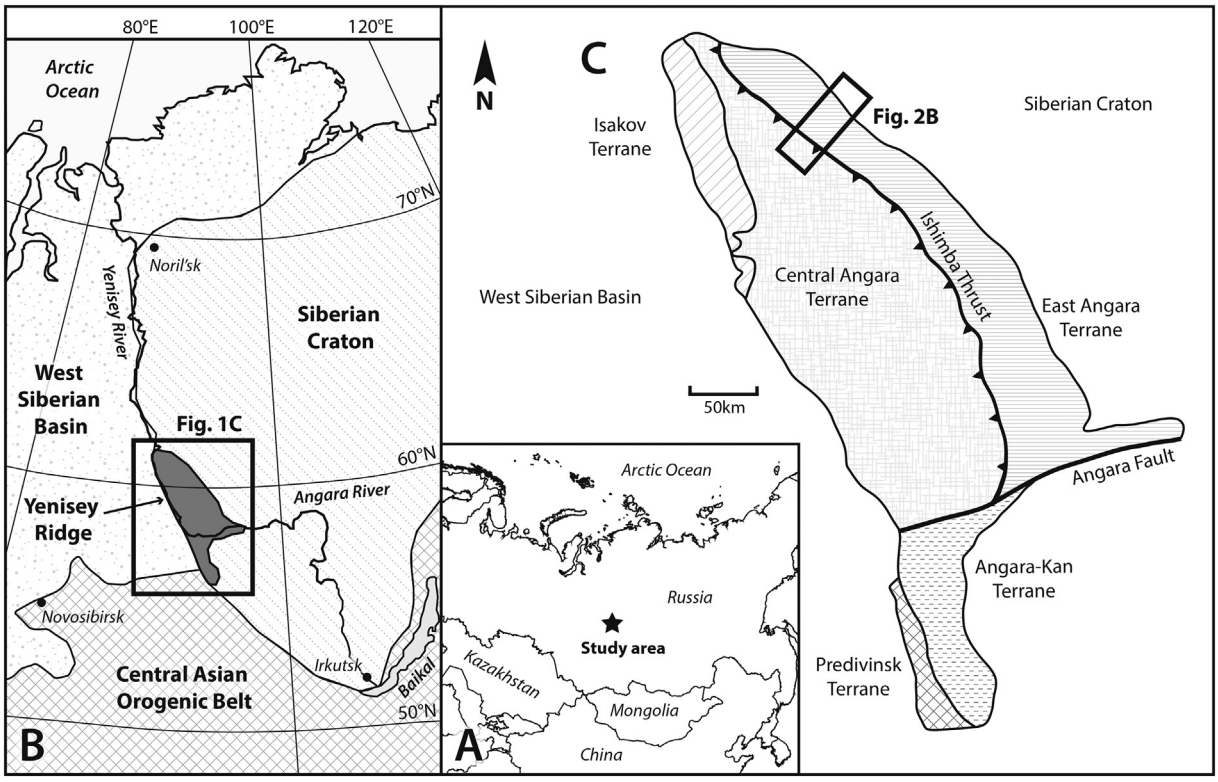

Fig. 1. A) The location of the study area within Eurasia, B) the position of the Yenisey Ridge with respect to the major geological features of Siberia (modified from Kuzmichev and Sklyarov, 2016), and C) terrane map of the Yenisey Ridge (Vernikovsky et al., 2016).

Siberia during the late Tonian (~760–720 Ma), while Likhanov et al. (2015) propose that the Central and Eastern Angara terranes were already part of the Siberian margin and experienced 'Grenvillian' orogenesis at ~1050–850 Ma. Kuzmichev and Sklyarov (2016) suggest a model where Central Angara was already a part of Siberia during the Neoproterozoic, and experienced the collision of an unidentified terrane at ~900–855 Ma. This model interprets the ~800–720 Ma magmatism as rift-related, in agreement with some of the other studies published in the area (e.g. Likhanov et al., 2014; Nozhkin et al., 2011).

2.2. Stratigraphy and samples

The Precambrian rocks that compose the Central and East Angara terranes in the north-eastern Yenisey Ridge can be divided into two categories: the metamorphosed Teya and Sukhopit Groups, and the essentially unmetamorphosed Cryogenian–Ediacaran Chingasan and Chapa Groups (Vernikovsky et al., 2016). Seven samples taken from throughout the stratigraphy were analysed in this study (Fig. 2). Priyatkina et al. (2016) published detrital zircon U-Pb data for four (YP1, 6, 8, and 21) of the seven samples that were analysed in this study. Note that samples YP1, 6, 8, and 21 in this study are named CHP1, 6, 8, and 21 in Priyatkina et al. (2016).

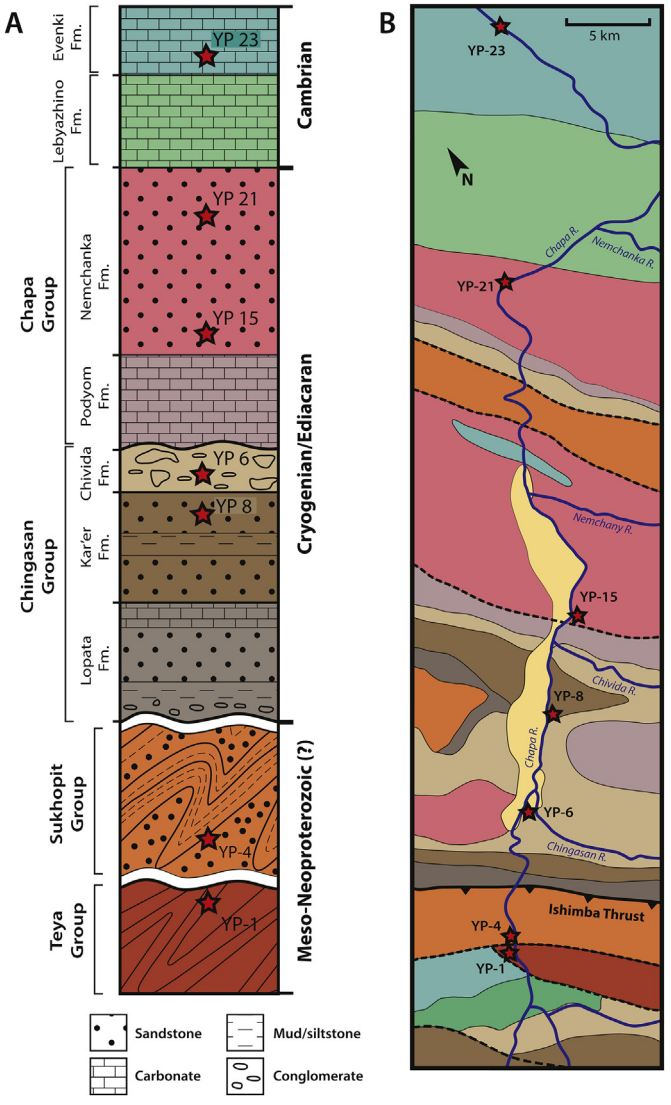

Fig. 2. A) Stratigraphy of the study area. Pattern corresponds to dominant lithology of unit. Stars represent approximate stratigraphic position of sample. Stratigraphic column modified after Priyatkina et al. (2016). B) Geological map of study area. Colours correspond to stratigraphic units in part A. Dashed lines are undifferentiated faults. Stars represent sample locations. Map modified after Pokrovsky et al. (2012).

Two of the studied samples (YP1, 4) are from the Central Angara terrane, whereas the remaining samples are from the East Angara terrane. The Meso- to Neoproterozoic stratigraphy is well studied in the East Angara terrane, where the sedimentary rocks are mildly deformed, unmetamorphosed to slightly metamorphosed, and are not intruded by granites (Mel'nikov et al., 2005; Pokrovsky et al., 2012). The relationships between local formations in the East Angara terrane are well documented. In contrast, the rocks of the Central Angara terrane are highly deformed and variably metamorphosed, with unclear correlations to the East Angara sedimentary succession (Vernikovsky et al., 2016 and references therein).

The Teya Group is exposed in the Central Angara terrane, where is it intruded by granites and has experienced greenschist to most typically amphibolite/epidote–amphibolite facies regional metamorphism (Nozhkin et al., 2012). It is composed of a variety of metamorphic rocks including gneisses, schists, quartzites, amphibolites, and marbles that are interpreted to have sedimentary protoliths (Nozhkin et al., 2012). The Palaeoproterozoic Penchenga Formation of the Teya Group consists mostly of gneisses and crystalline schists, with some marbles and quartzites (Nozhkin et al., 2012). The Penchenga Formation is unconformably overlain by the Korda Formation of the Sukhopit Group (Nozhkin et al., 2012). Sample YP1 was taken from a paragneiss of the Penchenga Formation.

Rock units assigned to the Sukhopit Group are exposed in both the Central And East Angara terranes, but the correlation of these rocks are questionable (Vernikovsky et al., 2016 and references therein). The Sukhopit Group is composed of sandstones, conglomerates, and shales, with some carbonate layers alternating with clastic sedimentary rocks in the central and upper part of the group (Vernikovsky et al., 2016). The basal conglomerate in the Korda Formation of the Sukhopit Group includes pebbles of the underlying Teya Group gneisses and schists (Nozhkin et al., 2012). The rocks of the Sukhopit Group experienced mostly greenschist facies regional metamorphism, with localised instances of amphibolite facies metamorphism in the lower parts of the group (Likhanov et al., 2007). The metamorphic grade in the lower Sukhopit Group increases with proximity to major thrusts, and this increase in grade is associated with changes in the style and intensity of deformation (Likhanov et al., 2007). In the Korda Formation, the local increase in metamorphic grade is characterised by the obliteration of widespread D1 isoclinal folds (Likhanov and Reverdatto, 2007). Furthermore, the lower part of the Korda Formation is marked by discontinuous volcanic bodies (Nozhkin et al., 2011), conglomerates, and quartzites (Nozhkin et al., 2009). Previous studies of the chemical and Sm-Nd isotopic composition of the fine-grained rocks from the Sukhopit Group and overlying units found that felsic rocks were the predominant source (Nozhkin et al., 2008; Nozhkin et al., 2009). Nozhkin et al. (2011) found that there was some contribution of juvenile material to the bottom and middle of the Sukhopit Group. $^{40}Ar/^{39}Ar$ biotite ages of 823–826 Ma from metapelitic sections of the Korda Formation are interpreted, by Likhanov et al. (2007), to represent the maximum age of greenschist metamorphism for this unit. Sample YP4 is from a fault-bound unit composed of isoclinally folded quartzite described as belonging to the Korda Formation.

The metamorphosed sedimentary rocks of the Central Angara terrane discussed above are intruded by several phases of granitic magmatism. The earliest of these granites intrudes the Teya Group and lower Sukhopit Group rocks, and provides the only firm age constraint on these sequences at ~880–860 Ma (Vernikovsky et al., 2016). The granitic Kalami pluton (875 ± 7 Ma; Vernikovsky et al. (2007)) intrudes rocks of the Korda Formation in the central part of the Yenisey Ridge (Varganov et al., 2010). Subsequent phases of magmatism in the Central Angara terrane occurred until around ~720 Ma (Vernikovsky et al., 2003). In the northern part of the Yenisey Ridge, the Cryogenian-Ediacaran Chingasan and Chapa Group sedimentary rocks

unconformably overlie the igneous intrusions and earlier metamorphic rocks (Vernikovsky et al., 2016). These rocks fill the Teya-Chapa sedimentary basin, and consist of unmetamorphosed sedimentary rocks with widely distributed red beds and locally distributed felsic and mafic volcanic rocks described by various authors as either a foreland or rift-related basin (e.g. Nozhkin et al., 2007).

The Chingasan Group is divided into three units: the Lopata, Kar'er and Chivida Formations.

The oldest formation in the Chingasan Group, the Lopata Formation, unconformably overlies the metamorphosed rocks of the Sukhopit Group and is mostly composed of fluvial conglomerates and sandstones, capped with stromatolitic dolomite (Nozhkin et al., 2007; Pokrovsky et al., 2012). The Kar'er Formation overlies the Lopata Formation and is composed of quartzose sandstone interbedded with some thin siltstone and mudstone layers. In the upper parts of the formation, some dolomite is also present (Pokrovsky et al., 2012). Sample YP8 was taken from a quartzose sandstone in the Kar'er Formation. The Chivida Formation contains a diamictite that has been interpreted by some as a Sturtian tillite (Pokrovsky et al., 2012), but is mostly composed of sandstone and siltstone with evidence of turbidite deposition (Nozhkin et al., 2007). Sample YP6 was taken from a sandstone in the Chivida Formation.

The sedimentary rocks of the Chapa Group unconformably overlie the Chingasan Group. The lower part of the Chapa Group, the Podyom Formation, is mostly composed of dolomites and limestones with some thin sandstone and siltstones (Pokrovsky et al., 2012). The Nemchanka Formation conformably overlies the Podyom Formation and is largely composed of clastic sedimentary rock (Pokrovsky et al., 2012). The lower sections are mostly finer sediments including mudstones and siltstones, while the middle is composed of red and pink sandstones with carbonate cement. The upper part is composed of coarse sandstones (Pokrovsky et al., 2012). Sample YP15 is taken from a sandstone in the lower part of the Nemchanka Formation, while YP21 is taken from a sandstone in the upper part up of the formation.

Conformably overlying the Chapa Group sedimentary rocks are Cambrian carbonates including the Lebyazhino and Evenki Formations. The base of the Lebyazhino Formation corresponds to the beginning of the Cambrian, according to palaeontological and isotopic data (Pokrovsky et al., 2012). The Evenki Formation is composed of various limestones and marls that are dated to the Middle-Upper Cambrian based on trilobite palaeontology (Pokrovsky et al., 2012). Sample YP23 is taken from a sandstone in the Evenki Formation.

3. Methods

Seven samples were taken in a linear transect across the north-eastern margin of the Yenisey Ridge, from the Central Angara terrane to the south-west of the Ishimba thrust, traversing the East Angara terrane, and ending with a final sample from the Evenki Formation on the Siberian platform (Fig. 2, Table 1). Apatite mineral separates from these samples were initially analysed for U and Pb isotopes on a NewWave UP213 ablation system coupled to an Agilent 7500 mass spectrometer as in Jepson et al. (2018). All samples were further investigated by reanalysis for 30 masses (Table 2), including U and Pb isotopes, trace elements and REEs guided by initial U-Pb results. The second round of analysis was carried out on a NewWave UP213 ablation system coupled to an Agilent 7900 mass spectrometer. Analytical parameters and isotopes measured can be found in Table 2. The analytical sequence in all cases consisted of two analyses of both the NIST SRM 610 glass (NIST610 hereafter; Hinton, 1999) and the Madagascar apatite (Thomson et al., 2012), plus a single analysis each of the Durango (McDowell et al., 2005) and Mt. McClure (Schoene and Bowring, 2006) apatites.

Table 2
Analytical parameters for LA-ICP-MS.

	1st round analysis	Trace element/REE reanalysis
Laser parameters		
Instrument	NewWave UP213	NewWave UP213
Washout	20s	20s
Background	30s	30s
Analysis duration	30s	30s
Laser repetition rate	5 Hz	5 Hz
Spot size	30 μm	30 μm
Energy	3.5 J/cm^2	3.5 J/cm^3
Carrier gas	700 mL/min He	700 mL/min He
Mass spectrometer		
Instrument	Agilent 7500	Agilent 7900
Isotopic and sample information		
Number of isotopes measured	11	30
Isotopes measured	^{29}Si, ^{35}Cl, ^{43}Ca, ^{44}Ca, ^{91}Zr, ^{204,206,207,208}Pb, ^{232}Th, ^{238}U	^{29}Si, ^{35}Cl, ^{43}Ca, ^{44}Ca, ^{51}V, ^{55}Mn, ^{88}Sr, ^{90}Zr, ^{139}La, ^{140}Ce, ^{141}Pr, ^{146}Nd, ^{147}Sm, ^{153}Eu, ^{157}Gd, ^{159}Tb, ^{163}Dy, ^{165}Ho, ^{166}Er, ^{169}Tm, ^{172}Yb, ^{175}Lu, ^{202}Hg, ^{204,206,207,208}Pb, ^{232}Th, ^{238}U

3.1. Apatite U-Pb

The apatite U-Pb method relies on the thermally activated volume diffusion of Pb within the crystal lattice of an apatite grain to provide information about its thermal history (Blackburn et al., 2011). Estimates of the closure temperature of the apatite U-Pb system range from 370 °C to >550 °C (Cochrane et al., 2014), although figures of 450–550 °C are more typical (e.g. Blackburn et al., 2011; Schoene and Bowring, 2007). Apatite U-Pb analysis was performed following the method described in Chew et al. (2014b). During apatite U-Pb analysis the Madagascar apatite primary reference material (Thomson et al., 2012) was measured repeatedly throughout the session to correct for instrumental drift and downhole fractionation, and the Mt. McClure (Schoene and Bowring, 2006) and Durango (McDowell et al., 2005) secondary reference materials were analysed as an accuracy check. Data reduction was performed using the 'VizualAge_UcomPbine' DRS in Iolite (Chew et al., 2014b; Paton et al., 2011). The often large amount of common (i.e. initial or non-radiogenic) Pb found in apatite necessitates the application of a correction to yield meaningful ages. Here we apply a ^{207}Pb based correction that depends on a known, or assumed, initial ^{207}Pb/^{206}Pb ratio (Gibson and Ireland, 1996), and apply this correction

Table 1
Sample locations and lithologies. IGSN: International Geo Sample Number.

Sample	IGSN	Latitude	Longitude	Lithology	Formation	Stratigraphic age
YP1	IEJAG0012	60.6826	91.8209	Paragneiss	Penchenga Formation, Teya Group	Paleoproterozoic
YP4	IEJAG0013	60.6839	91.8258	Quartzite	Korda Formation, Sukhopit Group (?)	Meso-Neoproterozoic (?)
YP6	IEJAG0014	60.7463	91.9246	Lithic sandstone	Chivida Formation, Chingasan Group	Cryogenian
YP8	IEJAG0015	60.7732	91.9966	Quartz sandstone	Kar'er Formation, Chingasan Group	Cryogenian
YP15	IEJAG0016	60.8111	92.0884	Red sandstone	Nemchan Formation, Chapa Group	Ediaracan
YP21	IEJAG0017	60.9876	92.2264	Red sandstone	Nemchan Formation, Chapa Group	Ediaracan
YP23	IEJAG0018	61.1080	92.3982	Lithic sandstone	Evenka Formation	Middle-upper Cambrian

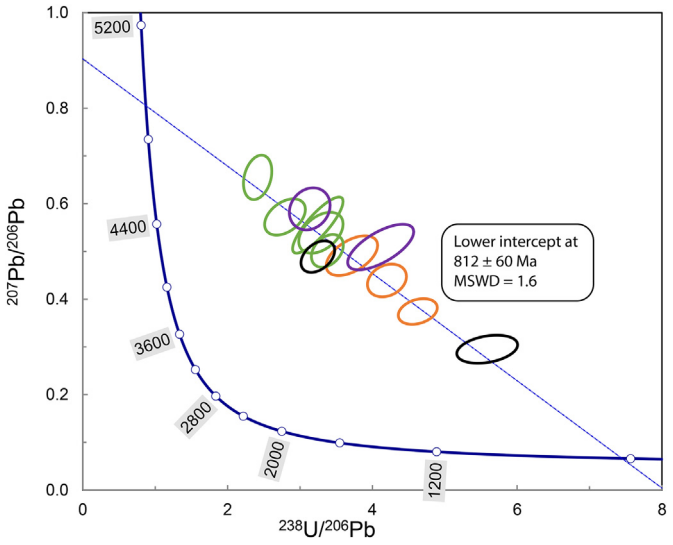

Fig. 3. Example from Sample YP8 of multiple U-Pb analyses of single apatite grains displayed on a Tera-Wasserburg diagram. Analyses of the same grain are identified by shared colour. Ellipses are plotted at 2σ. Concordia age values expressed in Ma.

to the standards according to the method described in Chew et al. (2014b). For the Mt. McClure apatite secondary standard, a weighted mean ^{207}Pb corrected $^{206}Pb/^{238}U$ age of 518.3 ± 6.1 Ma (MSWD = 1.4) was obtained, which is within uncertainty of the reference age of 523.51 ± 1.53 Ma (Schoene and Bowring, 2006).

Linear arrays of apatite U-Pb analyses in Tera-Wasserburg space were used to infer the initial $^{207}Pb/^{206}Pb$ ratio based on the $^{207}Pb/^{206}Pb$ (y-axis) intercept value for the array, which was subsequently used to perform the ^{207}Pb correction (Gibson and Ireland, 1996). Linear arrays of apatite U-Pb analyses on a Tera-Wasserburg plot are expected for cogenetic populations of apatites from a magmatic rock (e.g. Chew et al., 2014b; Gibson and Ireland, 1996). In the case of detrital apatite grains from a sedimentary rock, a population of analyses that produce a linear array in Tera-Wasserburg space is consistent with the existence of an age population. Multiple populations may be present and thus more complex distributions in Tera-Wasserburg space should be expected (e.g. Mark et al., 2016). In order to further investigate these populations, we performed further analysis of each grain to determine the trace element and REE composition. Cogenetic apatite grains have similar REE and trace element compositions, which can be used to discriminate between populations and define arrays in Tera-Wasserburg space. In addition, and where possible, multiple apatite U-Pb analyses of single grains were carried out. When the apatite grain has a variable amount of non-radiogenic Pb, multiple analyses define a linear array and further validate the use of a particular initial $^{207}Pb/^{206}Pb$ ratio (Fig. 3). When no clear linear array can be defined from the apatite data, the initial $^{207}Pb/^{206}Pb$ ratio predicted by the Stacey and Kramers (1975) Pb evolution model for the age of detrital zircon peaks was used as a substitute. This is described with reference to individual samples in Section 4.1. Repeated analyses of single grains are not included in the Kernel Density Estimator plots (KDE) (Vermeesch, 2012) used to display the relative abundance of different grain ages. Likewise, plots displaying the trace element and REE characteristics of particular samples only include the subset of analyses for which these elements were recorded. The tables that contain the subsets used in each of the plots can be found in the supporting information (Supplementary Tables A.1 and A.2).

3.2. Trace element and REE data

A selection of trace elements and REE were measured simultaneously to the acquisition of U and Pb isotopes with the LA-ICP-MS in order to geochemically characterise the apatite grains (Table 2). These elements were chosen based on their potential to provide information about the source rock from which a detrital apatite grain was derived (e.g. Belousova et al., 2002; Bruand et al., 2017; Dill, 1994; Fleischer and Altschuler, 1986; Henrichs et al., 2018; Morton and Yaxley, 2007).

Trace element and REE data reduction were performed using the 'X_Trace_Elements_IS' DRS in Iolite (Paton et al., 2011) as in Chew et al. (2016). Instrumental drift was corrected using NIST610 as the primary standard and ^{43}Ca was used as the internal elemental standard (Chew et al., 2014a). REE plots and discrimination diagrams were produced using an in-house R script.

4. Results

4.1. Apatite U-Pb

Sample YP1, taken from a paragneiss of the Penchenga Formation (Teya Group; Fig. 2) yielded 111 apatite U-Pb analyses that do not form clear linear arrays in Tera-Wasserburg concordia space (Fig. 4). For all analysed apatites, the Sr concentration is relatively low and consistent (~100–300 ppm). The significant data scatter without clear evidence for linear arrays impedes the calculation of common Pb regression lines. Therefore, for this sample, only a maximum and minimum apatite U-Pb age could be estimated at ~1790 Ma and ~850 Ma, respectively (Fig. 4). These ages are based on known geological constraints, explained in further detail in Section 5.2.1. The majority of U-Pb analyses lie between the arrays in Tera-Wasserburg defined by the Stacey and Kramers (1975) Pb evolution models for the aforementioned ages (Fig. 4). The continuous spread of data between those two arrays suggests open system behaviour of Pb, possibly as a result of a thermal perturbation.

Sample YP4, taken from a quartzite in the lower part of the Sukhopit Group (Fig. 2), yielded 78 apatite U-Pb analyses that form two distinct linear arrays on a Tera-Wasserburg plot (Fig. 4). A Palaeoproterozoic array of apatite analyses has a lower intercept age of 1810 ± 65 Ma (MSWD = 3.0) and is characterised by consistently elevated Sr concentrations (~500–650 ppm). A younger, Neoproterozoic array has a lower intercept age of 859 ± 24 Ma (MSWD = 2.1) and is characterised by apatites with significantly lower Sr concentrations (~250–350 ppm) compared to the Palaeoproterozoic array. The difference in Sr concentrations between the two apatite populations suggests that they are likely derived from sources with different lithologies (likely more mafic for the younger population (e.g. Jennings et al., 2011)). Three analyses (5% of the data) did not fall onto either array. After excluding analyses that represented multiple analyses of the sample grain, 53 unique apatite U-Pb ages were calculated following a ^{207}Pb correction based on the upper ($^{207}Pb/^{206}Pb$) intercept of the relevant common Pb regression line. A KDE plot (Fig. 4) of the corrected age data shows two peaks at the ages of the two lower intercept ages (~860 and ~1810 Ma).

Sample YP8, taken from a quartzose sandstone in the Kar'er Formation, yielded in total 79 apatite U-Pb analyses that form two linear arrays on a Tera-Wasserburg plot in addition to a number of other analyses that do not clearly form arrays. The older linear array has a lower intercept age of 1753 ± 33 Ma (MSWD = 3.0) and the apatites in this array are mostly characterised by low Sr concentrations

Fig. 4. Tera-Wasserburg (T-W) concordia diagrams and Kernel Density Estimator (KDE) plots of apatite U-Pb data from samples YP1, 4, 8, and 6 in stratigraphic order. Apatite U-Pb analyses for which trace element data were obtained are coloured according to their Sr contents on the T-W diagrams Ellipses are plotted at 2σ. On the T-W diagrams, the narrow-spaced dashed lines correspond to linear regressions through the apatite U-Pb data that were used to obtain an estimate of the initial $^{207}Pb/^{206}Pb$ ratio. The medium dashed lines are common Pb evolution lines defined by the Stacey and Kramers (1975) model for the age of detrital zircon U-Pb age peaks for that sample. The KDE plots show the distribution of zircon U-Pb ages from Priyatkina et al. (2016) in dashed outlines and pale grey fill, and the distribution of the ^{207}Pb corrected apatite U-Pb ages in solid outline and dark grey fill.

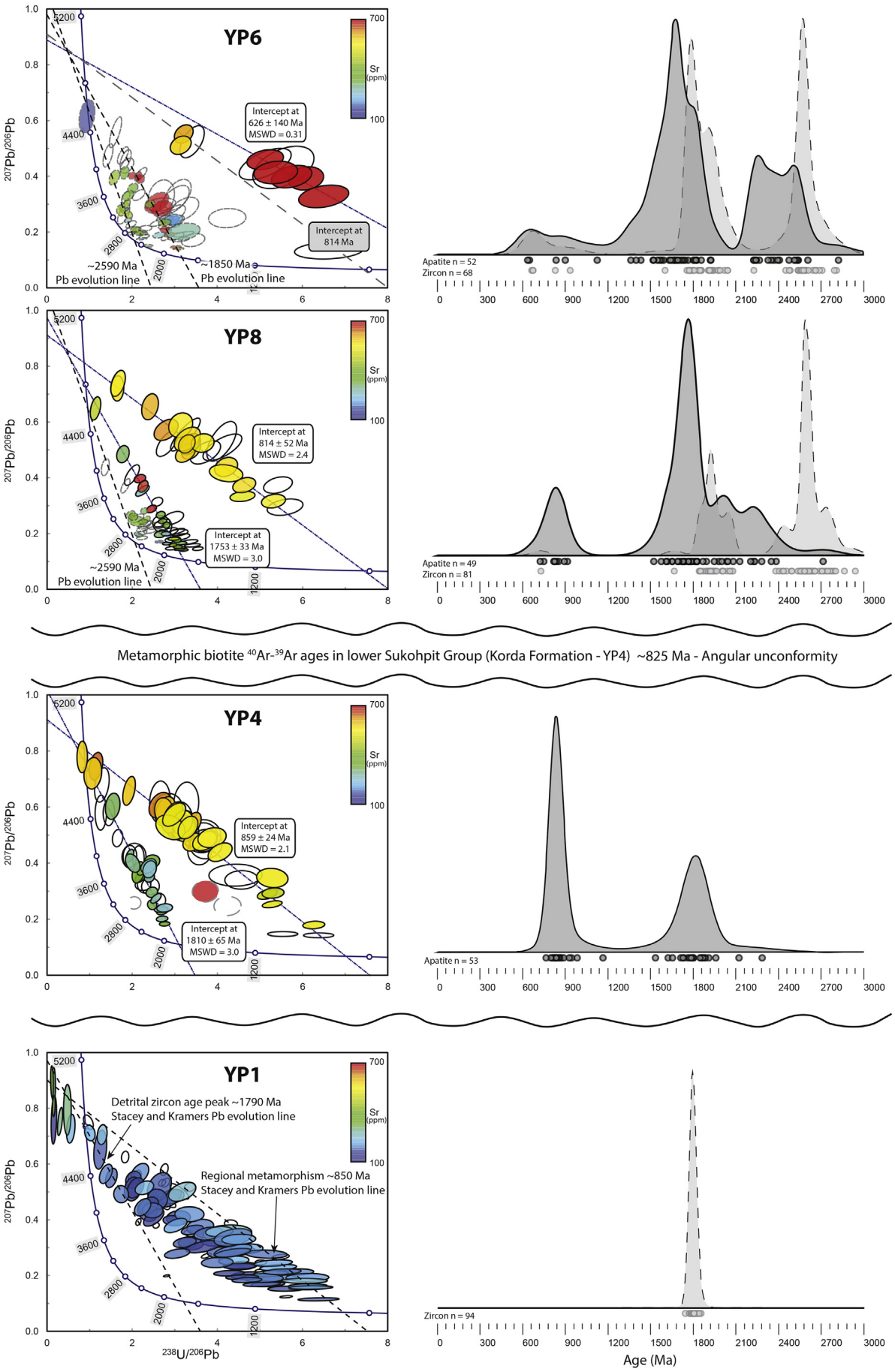
YP6
Intercept at
626 ± 140 Ma
MSWD = 0.31
Intercept at
814 Ma
~2590 Ma
Pb evolution line
~1850 Ma
Pb evolution line
Apatite n = 52
Zircon n = 68
YP8
Intercept at
814 ± 52 Ma
MSWD = 2.4
Intercept at
1753 ± 33 Ma
MSWD = 3.0
~2590 Ma
Pb evolution line
Apatite n = 49
Zircon n = 81
Metamorphic biotite 40Ar-39Ar ages in lower Sukohpit Group (Korda Formation - YP4) ~825 Ma - Angular unconformity
YP4
Intercept at
859 ± 24 Ma
MSWD = 2.1
Intercept at
1810 ± 65 Ma
MSWD = 3.0
Apatite n = 53
YP1
Detrital zircon age peak ~1790 Ma
Stacey and Kramers Pb evolution line
Regional metamorphism ~850 Ma
Stacey and Kramers Pb evolution line
Zircon n = 94
Sr (ppm)
207Pb/206Pb
238U/206Pb
Age (Ma)

(<450 ppm; three analyses from a single apatite grain yield anomalously high ~700 ppm Sr values). The younger linear array has a lower intercept age of 814 ± 59 Ma (MSWD = 2.4) and yields apatites with consistently higher Sr concentrations (>500 ppm). Hence, the two defined apatite populations are similar to those in sample YP4, likely reflecting different source lithologies. A cluster of analyses with apparently older ages than the oldest linear array are poorly defined in terms of initial $^{207}Pb/^{206}Pb$. These analyses were corrected using an initial $^{207}Pb/^{206}Pb$ ratio calculated from the Stacey and Kramers (1975) Pb evolution model for the age of the older zircon peak (~2590 Ma) from this sample. These analyses therefore produce ages of low accuracy and should be treated with caution. These apparent >1.8 Ga ages are absent in sample YP4. A KDE plot of the 49 unique apatite U-Pb ages from this sample shows two main peaks with ages similar to the two lower intercept ages, in addition to a tail of older ages from the ~1750 Ma peak (Fig. 4). This Palaeoproterozoic apatite peak is younger than the similar zircon U-Pb age peak, while the Neoproterozoic apatite and zircon peaks overlap closely.

Sample YP6 from the Chivida Formation yielded 79 apatite U-Pb analyses that are highly scattered and do not form any clear linear arrays. Repeated analyses of the two youngest grains produced seven analyses that form a linear array with consistently high Sr concentrations (>700 ppm) and a lower intercept age of 629 ± 140 Ma (MSWD = 0.31). Four analyses (with slightly lower Sr concentrations of ~500 ppm) are consistent with the Neoproterozoic linear arrays from YP4 and YP8. The remaining analyses appear to be significantly older (mostly Palaeoproterozoic) and do not form clear linear arrays. The apparently older apatite analyses were corrected using an initial $^{207}Pb/^{206}Pb$ ratio calculated from the Stacey and Kramers (1975) Pb evolution model for the age of the Palaeoproterozoic–Neoarchaean zircon age peak from this sample. As in YP8, the grains corrected using this approach should be treated with caution. This approach yielded 52 unique apatite U-Pb ages that resemble in terms of proportions of ages the zircon U-Pb age distribution when displayed on a KDE plot (Fig. 4). The apatite U-Pb age peaks tend to be slightly younger than the zircon age peaks.

Two samples were taken from the Nemchanka Formation. YP15 yielded 67 apatite U-Pb analyses that form two linear arrays (Fig. 5). The older (Palaeoproterozoic) array has a lower intercept age of 1828 ± 110 Ma (MSWD = 2.4). The younger (Neoproterozoic) array has a lower intercept age of 730 ± 45 Ma (MSWD = 6.5). Sr concentrations for the apatites in the younger array are highly variable, while for the older array, they are rather consistent at ~200–450 ppm. The 47 unique apatite U-Pb ages from this sample form two peaks at ~730 Ma and ~1830 Ma on a KDE plot.

YP21 yielded 60 apatite U-Pb analyses that form two distinct Tera-Wasserburg linear arrays with lower intercepts at 1761 ± 50 Ma (MSWD = 4.6) and 839 ± 32 Ma (MSWD = 4.4). Sr concentrations are rather variable in both populations. Ten analyses did not belong to either array and were corrected as in previous samples using an initial $^{207}Pb/^{206}Pb$ ratio calculated from the age of the oldest detrital zircon peak from this sample. The 43 unique apatite U-Pb ages from this sample form three peaks at ~840 Ma, ~1850 Ma, and ~2500 Ma, similar to the ages of the zircon U-Pb peaks.

The Evenka Formation (YP23) yielded 57 apatite U-Pb analyses that form a linear array on a Tera-Wasserburg plot with a lower intercept of 745 ± 37 Ma (MSWD = 8.6). The Sr contents of these grains are generally low with only one high Sr (>500 ppm) apatite grain. The 48 unique apatite U-Pb ages from this sample form a peak at ~760 Ma on a KDE plot.

4.2. Trace element and REE data

4.2.1. Chondrite-normalised REE plots

The chondrite-normalised REE plots for sample YP1 show identical patterns for all grains, suggesting that all analysed apatites define a single trace element population. The apatites from this sample yield a strong negative Eu anomaly, and a fairly flat REE profile, with slight depletion of HREE relative to LREE and MREE (Fig. 6).

In contrast, three apatite populations can be defined in sample YP4, based on the differences in their REE patterns. The first apatite population is comprised of all analysed young (Neoproterozoic) U-Pb ages and is characterised by moderate enrichment in LREEs without significant or systematic Eu anomalies. The second population is defined by three old (Palaeoproterozoic) apatites. Their REE patterns are similar to those for the apatites in population one (enriched LREEs) but show an additional negative Eu anomaly. All other Palaeoproterozoic apatites belong to population three, and are moderately to strongly depleted in LREEs (depleted = $(Ce/Yb)_{cn} < 1$) with generally positive Eu anomalies.

Samples YP6 and YP8 are similar to one another in that the majority of the grains (with the exception of one analysed old grain from YP8) are moderately enriched in LREEs. Generally, there is a fair amount of diversity in the REE profiles of older grains, with some preserving significant Eu anomalies. In contrast, younger grains have quite uniform REE profiles across all three samples and do not record major positive or negative Eu anomalies.

The REE profiles of samples YP15, YP21, and YP23 are markedly different from those collected below the unconformity defining the base of the Chapa Group (Figs. 2 and 7). The majority of grains in the youngest three samples have flat REE profiles, while some populations are slightly enriched in LREE or MREE. Older grains tend to have no Eu anomaly, or only minor positive or negative anomalies. A large proportion of younger grains have large negative Eu anomalies.

4.2.2. La/Nd vs La + Ce/ΣREE discrimination diagrams

The analysed apatites from YP1 fall into the acidic field on the La/Nd vs La + Ce/ΣREE plot (Fig. 6). In contrast, the young grains from YP4, YP8, and YP6 all have high La/Nd and La + Ce/ΣREE ratios, plotting in the mafic to intermediate field. Older grains from YP4 are mostly very acidic, while the older grains from YP8 and YP6 have a wider range of values (mostly plotting between acidic and intermediate compositions). Only a few grains from each sample fall into the alkaline field.

The majority of apatites from YP15, YP21, and YP23 fall into the acidic field, while a few grains with higher La/Nd and La + Ce/ΣREE ratios fall into either the intermediate-mafic or alkaline fields (Fig. 6).

4.2.3. Th-U plots

All of the apatites analysed for sample YP1 have higher Th concentrations than U concentrations, and fall between the 1:1 and 10:1 Th-U lines (Fig. 8). The apatites tend to have high to very high values of both Th and U (4–150 ppm U, 20–500 ppm Th). The young (Neoproterozoic) apatites from YP4 tend to have Th > U and fall between the 1:1 and 10:1 Th-U ratio lines. In contrast, the older analysed apatites from sample YP4 generally plot on the Th depleted side of the 1:1 or even 1:10 Th-U lines. In samples YP6 and YP8, young grains consistently have Th > U, while older grains fall on both sides of the 1:1 line, and have highly variable Th and U concentrations (<1 ppm to >100 ppm).

Samples from above the Chingasan–Chapa unconformity (i.e. YP15, YP21, and YP23) have less clear patterns in terms of the distributions of age populations. Both young and old grains in all samples fall on both sides of the 1:1 line, but in general, apatites from these samples more often have Th < U and are sometimes extremely depleted in Th.

5. Discussion

The trace element and REE data obtained in this study provide evidence for a significant change in the character of the source rocks at the time of the Chingasan Group (YP6, 8) – Chapa Group (YP15, 21) unconformity. This is seen most obviously in the Neoproterozoic populations, which have similar ages on both sides of the unconformity, but differ significantly in REE and trace element composition (Fig. 9).

Studies of apatite geochemistry in terms of provenance discrimination (e.g. Belousova et al., 2002; Bruand et al., 2017; Dill, 1994;

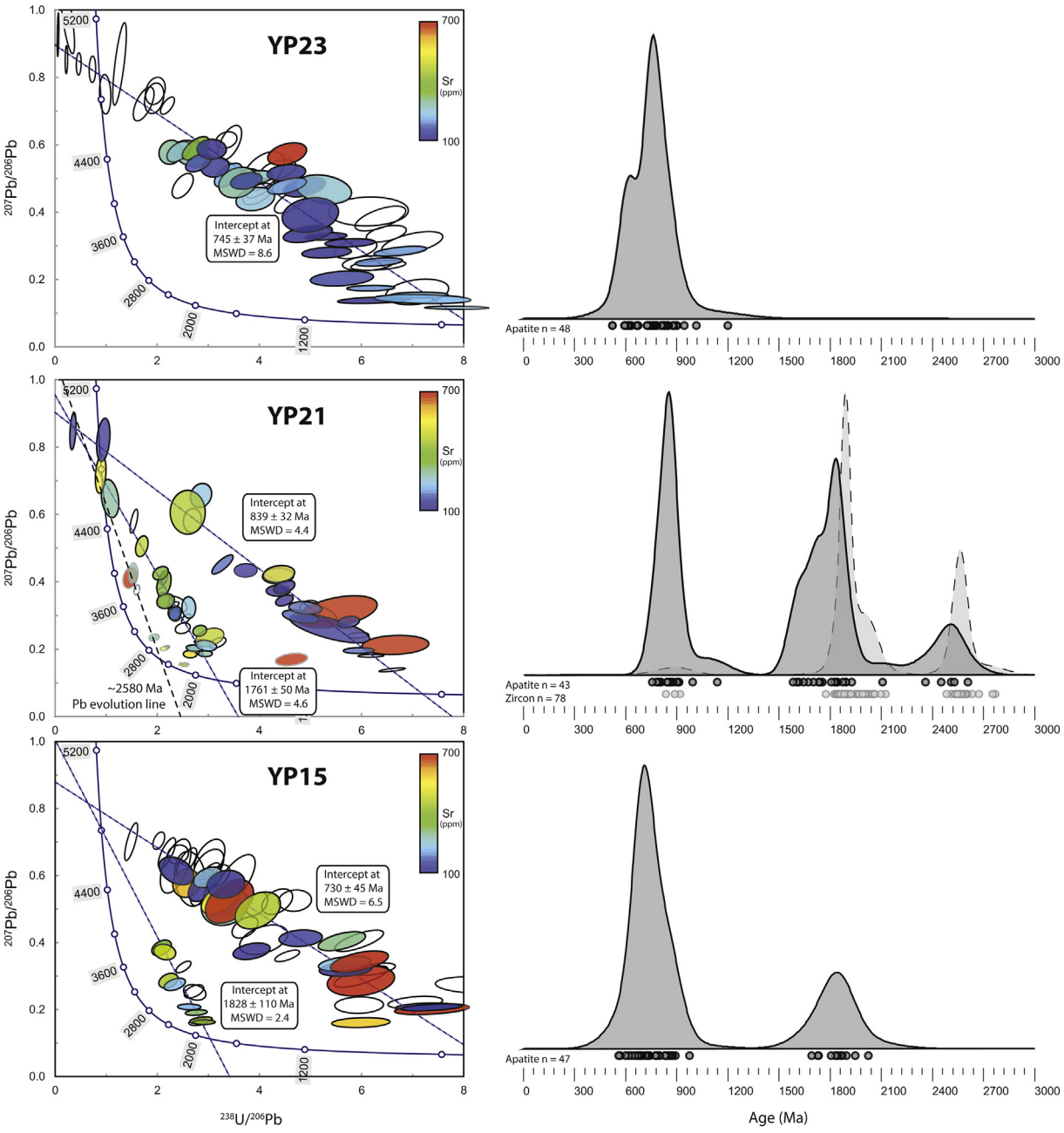

Fig. 5. Tera-Wasserburg (T-W) concordia diagrams and Kernel Density Estimator (KDE) plots of apatite U-Pb data from samples YP15, 21, and 23 in stratigraphic order. Apatite U-Pb analyses for which trace element data were obtained are coloured according to their Sr contents on the T-W diagrams. Ellipses are plotted at 2σ. On the T-W diagrams, the narrow-spaced dashed lines correspond to linear regressions through the apatite U-Pb data that were used to obtain an estimate of the initial $^{207}Pb/^{206}Pb$ ratio. The medium dashed lines are the common Pb evolution lines defined by the Stacey and Kramers (1975) model for the age of detrital zircon U-Pb age peaks for that sample. The KDE plots show the distribution of zircon U-Pb ages from Priyatkina et al. (2016) in dashed outlines and pale grey fill, and the distribution of the ^{207}Pb corrected apatite U-Pb ages in solid outline and dark grey fill.

Fleischer and Altschuler, 1986; Morton and Yaxley, 2007) have produced many recommendations regarding the categorisation of detrital apatite grains. In this study we have adopted a number of strategies from the literature, described below, in order to understand the geochemical signatures recorded in the analysed apatite grains.

5.1. Geochemical provenance discrimination of detrital apatite grains

The La/Nd vs La + Ce/ΣREE plot was proposed by Fleischer and Altschuler (1986) as a tool to categorise detrital apatites. This discrimination diagram has three fields that are defined by host rocks with acidic, intermediate-mafic, or alkaline chemistries. The behaviour of REEs in apatite is controlled by both the host rock composition and the degree of fractionation (Belousova et al., 2002; Morton and Yaxley, 2007). Alkaline rocks and less fractionated mafic rocks tend to be enriched in LREEs (Morton and Yaxley, 2007), while flat to LREE depleted REE profiles are characteristic of S-type and felsic I-type peraluminous granites (Sha and Chappell, 1999). LREE depletion is frequently attributed to the growth of monazite prior to the crystallization of apatite in these magmas. Extreme LREE depletion (extending to Gd) is found in apatite from strongly fractionated granites and in apatite grown under metamorphic conditions, as the result of competition for these elements by minerals such as allanite, epidote and feldspar (Chu et al., 2009; Henrichs et al., 2018).

The presence of a negative Eu anomaly (Eu/Eu*) in apatite is normally interpreted as the result of competition for Eu^{2+} by the

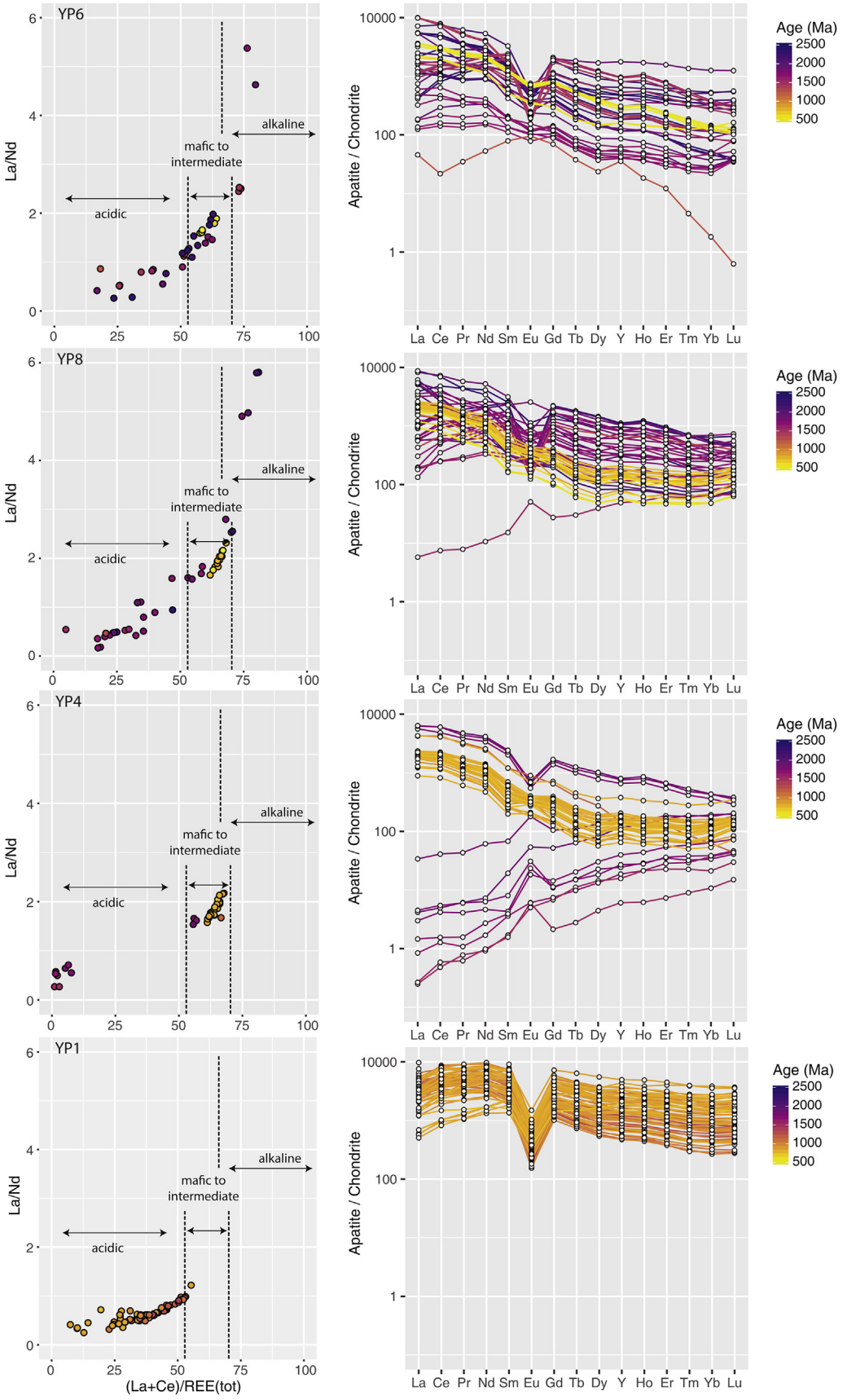

Fig. 6. La/Nd vs La + Ce/ΣREE diagrams from Fleischer and Altschuler (1986) and chondrite normalised REE profile plots of samples YP1, 4, 8, and 6. Cl chondrite values from Sun and McDonough (1989). Analyses are coloured according to their ^{207}Pb corrected apatite U-Pb age. Note that not all grains were able to be reanalysed for trace elements and REEs so the proportions of each age population are not the same as on KDE plots.

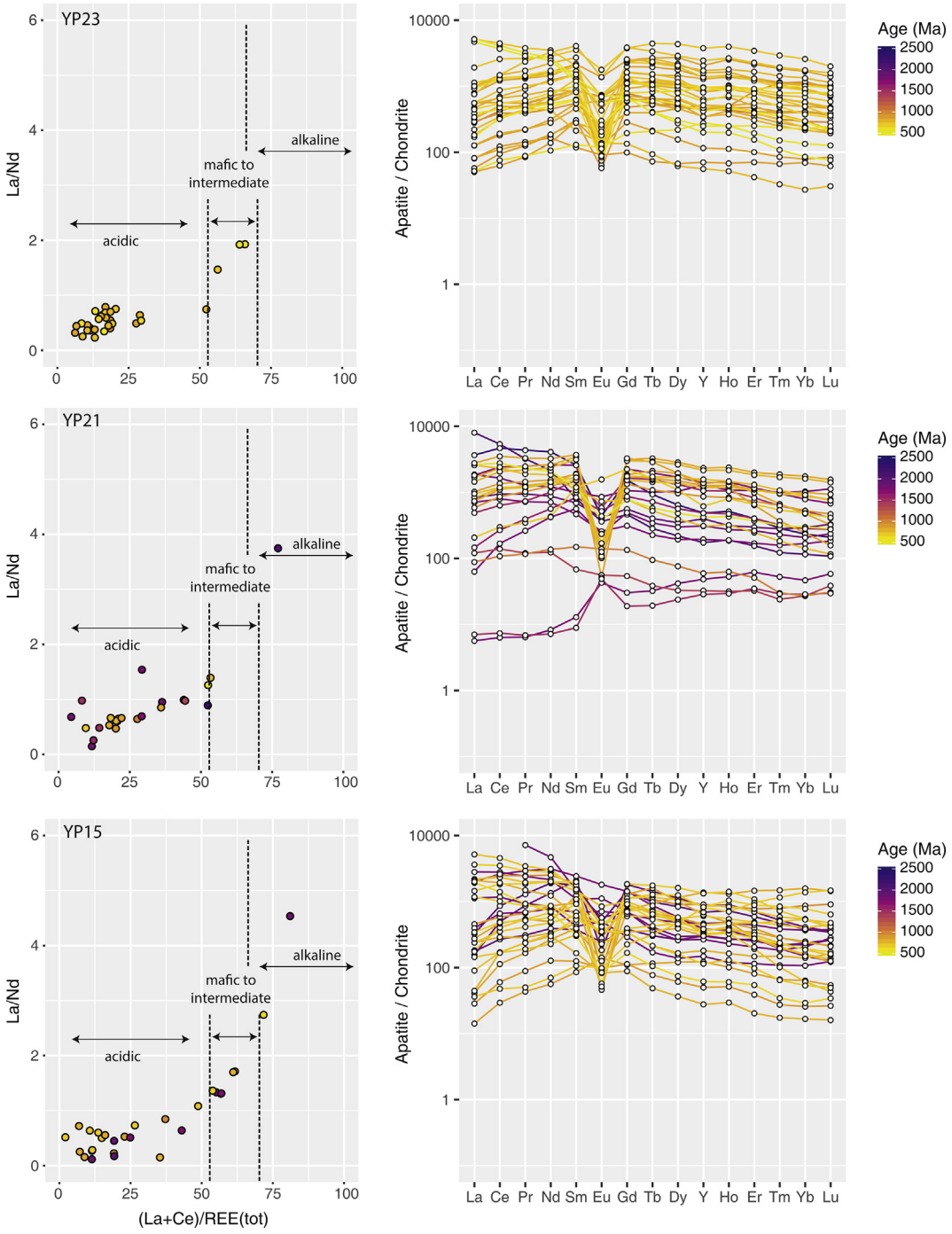

Fig. 7. La/Nd vs La + Ce/ΣREE diagrams from Fleischer and Altschuler (1986) and chondrite normalised REE profile plots of samples YP15, 21, and 23. Cl chondrite values from Sun and McDonough (1989). Analyses are coloured according to their ^{207}Pb corrected apatite U-Pb age.

crystallization of feldspar (Belousova et al., 2002) and so is associated with relatively fractionated rocks. The lack of significant Eu anomalies, either positive or negative, is a common feature of apatites from less fractionated mafic rocks (Chu et al., 2009). Positive Eu anomalies in apatite cannot be created by fractionation and so are diagnostic of a pre-existing positive Eu anomaly in the parent magma (Chu et al., 2009).

The negative correlation between the Sr content of a magmatic apatite and the SiO_2 content of the rock in which it formed (Bruand et al., 2016; Bruand et al., 2017; Jennings et al., 2011) can be used to estimate the whole rock SiO_2 of the source rock for a detrital grain (e.g. Bruand et al., 2017). Apatites from intermediate-mafic rocks tend to have higher Sr contents (~ > 400 ppm) than those from felsic rocks.

The Th—U binary plot was first used by Dill (1994) as a detrital apatite discrimination plot. The depletion of Th relative to U is usually attributed to the crystallization of monazite, which has a strong affinity for Th (Spear and Pyle, 2002). Th depletion may be seen in apatite from strongly fractionated rocks where monazite crystallizes before apatite, or in metamorphic apatite from pelitic rocks that may also face competition with monazite or epidote in a similar fashion (Spear and Pyle, 2002). In general, grains on the Th < U side of the line may indicate a more highly evolved source or a metamorphic origin (Sha and Chappell, 1999; Spear and Pyle, 2002). Henrichs et al. (2018) found that Th depletion in low- to medium-grade metamorphic apatite from a variety of protoliths was nearly ubiquitous, and also observed Th

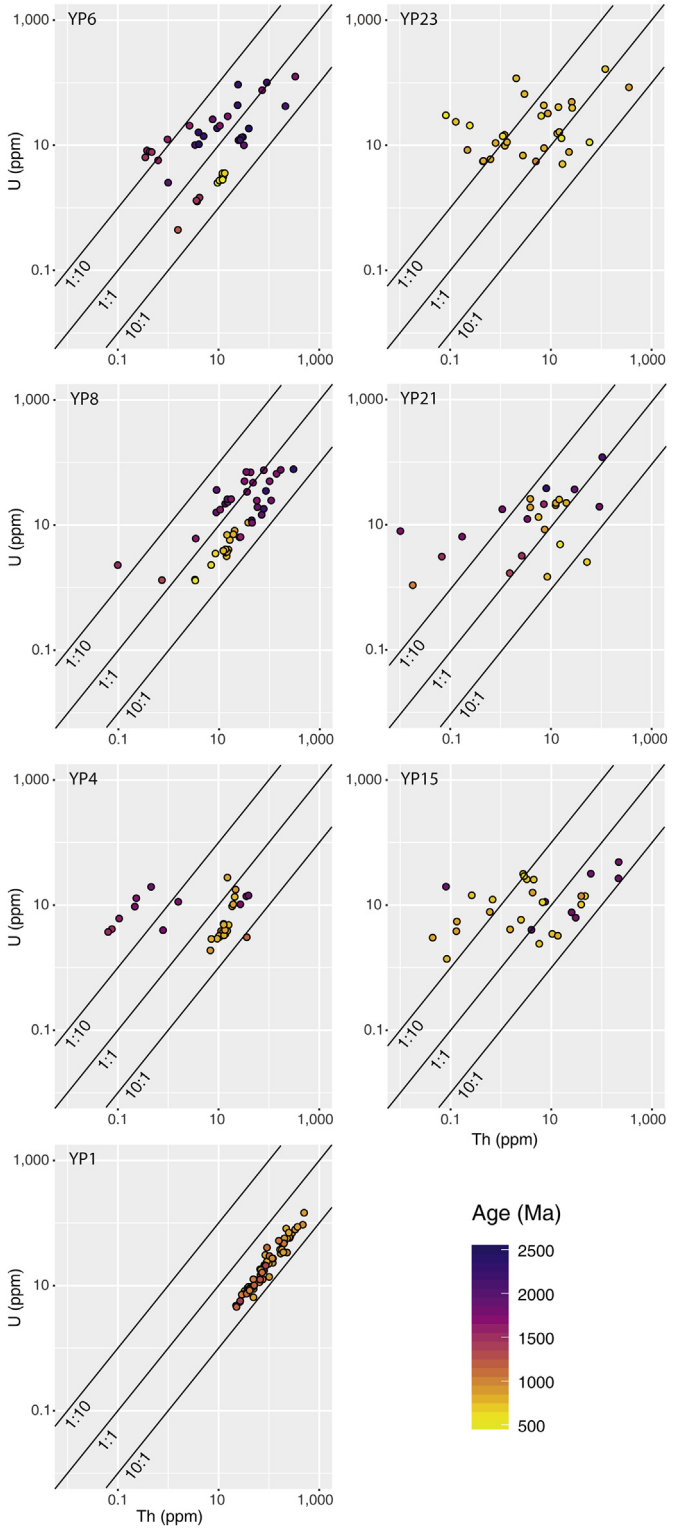

Fig. 8. Th-U binary plots (Dill, 1994) of grains from all analysed samples, coloured according to ^{207}Pb corrected apatite U-Pb age. Diagonal lines show Th-U ratios of 1:10, 1:1, and 10:1.

depleted metamorphic overgrowths around high Th cores interpreted to be of detrital igneous origin.

In general, metamorphic apatite from low- to medium-grade metapelites and metabasites can be identified by very low Th and LREE concentrations, and are often also low in U (Henrichs et al., 2018; Spear and Pyle, 2002). In addition to having distinct trace element and REE characteristics, Henrichs et al. (2018) found that low-grade metamorphic apatites from a wide range of protoliths and terranes were typically so poor in U that they were undateable using the U—Pb LA-ICP-MS method.

5.2. Interpretation of apatite U-Pb data in terms of detrital populations

5.2.1. Below the Chingasan–Chapa unconformity

The oldest unit sampled in this study, the Penchenga Formation (YP1), was found in previous work to have a single, well-defined population of zircons (n = 94 < 5% discordant ages) with a peak at ~1790 Ma (Priyatkina et al., 2016). The youngest single grain (YSG) age is 1743 ± 22 Ma. This is consistent with previous late Palaeoproterozoic estimates of the timing of deposition based on 1660–1680 Ma K-Ar mica ages from microschists (Volobuev et al., 1976 as cited in Nozhkin et al., 2012). Our new apatite U-Pb data for this sample do not record a clear linear array but rather a wide band of analyses in Tera-Wasserburg space, with apparent scatter along the ^{238}U/^{206}Pb axis of the concordia plot (Fig. 4). Sr and REE patterns are consistent for all grains in sample YP1, suggesting a single apatite population (in terms of trace element geochemistry) with felsic source rock characteristics (Fig. 6). The lack of well-defined linear arrays shown by the apatite U-Pb analyses probably does not relate to different detrital sources but likely reflects open system Pb behaviour partially to completely resetting the U-Pb system, probably by reheating at temperatures of at least ~450–550 °C (Blackburn et al., 2011). A maximum age of ~1790 Ma and minimum age of ~850 Ma was estimated based on the spread of apatite U-Pb analyses and the geological history of the sample. We interpret the maximum and minimum apatite U-Pb ages to represent the timing of the original detrital age of the population prior to partial reset (based on zircon U-Pb age of ~1790 Ma) and the time of regional metamorphism in the Yenisey Ridge at ~850 Ma, respectively (Likhanov et al., 2008). Partial to complete resetting of the apatite U-Pb system via thermally activated volume diffusion of Pb is consistent with the epidote-amphibolite to amphibolite facies metamorphic conditions that the Penchenga Formation is thought to have experienced at ~850 Ma (Likhanov et al., 2008). The high Th values (Fig. 8) suggest that the apatite is unlikely to have formed under metamorphic conditions (Henrichs et al., 2018; Spear and Pyle, 2002), and consequently the spread of old to young apatite ages are interpreted as the result of the thermally activated volume diffusion of Pb rather than recrystallization or new growth.

Sample YP4 yielded no dateable zircons. The apatites analysed from this sample produced two well-defined age populations. The younger, Neoproterozoic, age population contains 53% of the apatite grains and has an age of 859 ± 24 Ma (MSWD = 2.1). The Palaeoproterozoic age component contains 43% of grains and has an age of 1810 ± 65 Ma (MSWD = 3.0). The remaining three grains do not fall onto either array and are treated as outliers and not discussed further. The two populations are clearly distinguished by their Sr contents (Fig. 4) and REE profiles (Fig. 6). These different geochemical signatures suggest that the two apatite U-Pb populations reflect different sources rather than partial resetting (discussed further in Section 5.2.2). The relatively high Sr (>500 ppm) content of the young apatites from sample YP4 suggest that it is more likely that the source of these grains had an intermediate–mafic composition (Bruand et al., 2017). These grains are also characterised by a lack of significant Eu anomalies, either positive or negative, a common feature of apatites from less fractionated rocks (Chu et al., 2009). This interpretation is also consistent with the classification of the source of young grains as intermediate-mafic by the La/Nd vs La + Ce/ΣREE discrimination diagram (Fig. 6). These Neoproterozoic grains are broadly characterised by an enrichment in LREE and Th, high Sr, and a lack of significant Eu anomalies.

The Palaeoproterozoic age component in YP4 is dominated by apatites that are strongly depleted in LREE and have a positive Eu anomaly (Fig. 6). This level of LREE depletion is associated with strongly fractionated granitic source rocks or growth under metamorphic conditions

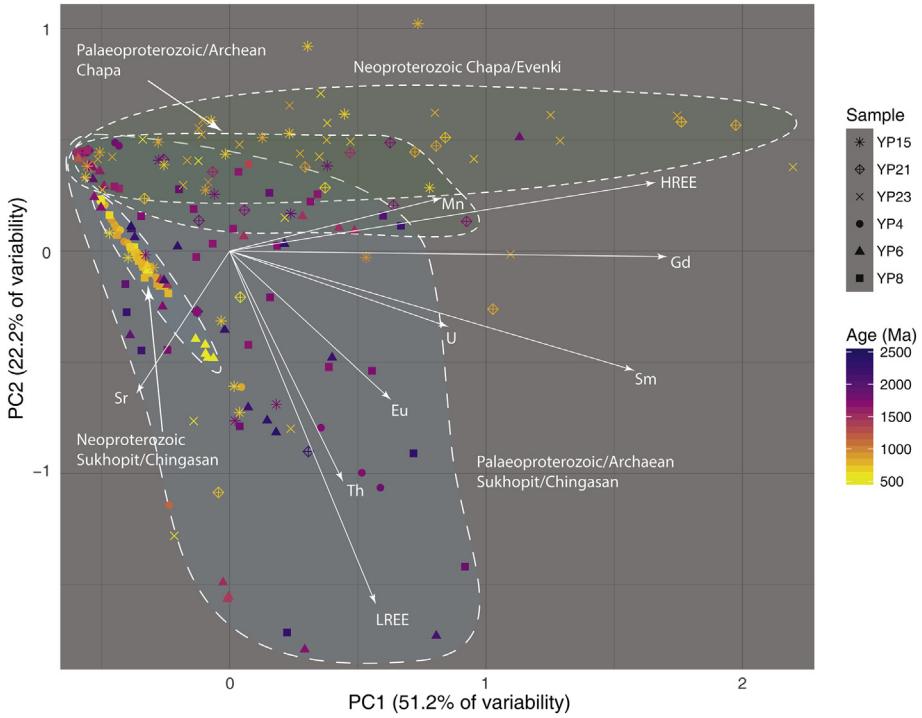

Fig. 9. Biplot of the results of (scaled) Principal Component Analysis (Oksanen et al., 2017) of geochemical data (19 elements) obtained for detrital apatite grains from six samples in the Yenisey Ridge. Principal Component 1 (PC1) plotted against PC2 explains >73% of the variability in the data. Elemental vectors (white arrows) point in the direction most similar to the variability in elemental concentration. For clarity, many of the REEs with similar vectors are depicted with a representative vector in the case of LREE (La, Ce, Pr, Nd) and HREE (Tb, Dy, Y, Ho, Er, Tm, Yb, Lu). The green zones are the areas interpreted to contain most of the grains from samples YP15, 21, and 23. The blue zones are those that are interpreted to contain most of the grains from YP4, 8, and 6. These zones are further subdivided into the Neoproterozoic and Palaeoproterozoic/Archaean age populations. YP1 was not included as this sample is interpreted to have been significantly affected by metamorphism and may not reflect a detrital signature. (For interpretation of the references to colour in this figure legend, the reader is referred to the web version of this article.)

(Chu et al., 2009; Henrichs et al., 2018; Spear and Pyle, 2002). Their relatively low (<350 ppm) Sr concentrations are consistent with a felsic source. The positive Eu anomaly in apatite cannot be created by fractionation so must be the result of a pre-existing positive Eu anomaly in the parent magma (Chu et al., 2009). A minor component of the Palaeoproterozoic population is enriched in LREE (including a negative Eu anomaly) and has an intermediate–mafic La/Nd vs La + Ce/ΣREE signature.

Both samples from the Chingasan Group (YP8 and YP6) have apatite and zircon U-Pb data. Apatite and zircon record quite different U-Pb age distributions in YP8. Sample YP8 yielded 81 < 5% discordant zircon U-Pb ages that range between 728 ± 18 Ma and 2941 ± 14 Ma, with major peaks at ~1870 and ~2580 Ma (Priyatkina et al., 2016). The YSG age is 728 ± 18 Ma. Tonian ages are found in both sets of data, but while this population represents 16% of the apatite data, only a single zircon of this age was found. The majority of the apatite U-Pb data (~65–75%) falls into a late Palaeoproterozoic (~1700–1800 Ma) population. The remaining 10–20% of the apatite U-Pb data belongs to a poorly defined group that do not clearly belong to a linear array but are clearly older than ~1800 Ma. In contrast, the largest population of zircon ages (65%) is early Palaeoproterozoic to Neoarchaean in age (>2400 Ma). The relative lack of old apatite ages in comparison to the proportion of old zircon ages may reflect the increasing chance that old source rocks will have experienced subsequent heating and metamorphism that would reset the apatite U-Pb ages. Alternatively, the relatively high abundance of older zircon ages could also represent the recycling and concentration of old zircons through several sedimentary cycles rather than being a reflection of primary provenance (e.g. Andersen et al., 2016). The geochemical signatures of the Neoproterozoic populations in YP6 and YP8 are similar to YP4, characterised by elevated Sr concentrations (>500 ppm) in combination with La/Nd ratios and REE patterns that suggest a mafic to intermediate source (Fig. 6). This magmatic composition is less likely to produce zircon and may explain the discrepancy between the abundance of Neoproterozoic apatite and zircon ages in YP8.

Older (Palaeoproterozoic or Archaean) apatite grains from YP6 and YP8 have a broad range of trace element and REE characteristics, and do not form such clear populations as those grains discussed thus far. They are variably enriched in LREE and Th, with a significant proportion of analyses falling on either side of the Th/U 1:1 line, and a similarly wide distribution in terms of LREE enrichment as seen on the REE plots and the La/Nd vs La + Ce/ΣREE discrimination diagram. Large negative Eu anomalies are present in a minority of older grains, but small or non-existent anomalies are most common. The Sr contents of most of these grains are low (<400 ppm), with only a few grains that have high (>700 ppm) concentrations.

Sample YP6 yielded 68 < 5% discordant zircon U-Pb ages that range from 663 ± 13 to 2807 ± 27 Ma, with a major population at 1800–2000 Ma and an older peak at ~2590 Ma (Priyatkina et al., 2016). The YSG age is 663 ± 13 Ma. The apatite U-Pb data from YP6 are difficult to interpret due to the highly scattered analyses that do not neatly fall into linear arrays. Trace element characteristics in the different populations are similar to those in YP8, particularly in terms of the high Sr of the younger population and the broadly similar REE profiles. The apatite U-Pb age distribution produces peaks somewhat younger than the zircon age distribution, but the proportion of apatite and zircon grains in each age group is much more similar than for other samples. This is indicative of a broad trend from YP4 through YP8 and YP6, where the proportion of Neoproterozoic apatites decreases as the proportion of >2000 Ma apatites increases. This trend may reflect either the depletion of the young apatite source or an increase in the volume of sediment from a source of older apatites over time.

5.2.2. Implications for the depositional age of the Sukhopit Group

Previous work has generally assumed that the sedimentary rocks of the Sukhopit Group were deposited during the Mesoproterozoic (e.g. Likhanov et al., 2007). The presence of a significant population of apatites with a lower intercept age of ~860 Ma in sample YP4 calls into doubt the correlation of the metamorphic rock unit that this sample was taken from, as this result implies the unit is younger than the Kalami pluton (875 ± 7 Ma; Vernikovsky et al. (2007)) that cuts rocks of the Korda Formation elsewhere in the Yenisey Ridge (Varganov et al., 2010). The combination of multiple data sets in our study lends strong evidence to the interpretation of a Neoproterozoic depositional age for sample YP4. The grains that appear to belong to this population all have very similar trace element and REE chemistry, plotting in a tight grouping on the discrimination diagrams and on the REE plot (Fig. 6, Fig. 8). This is also seen in the Sr concentrations plotted on the concordia plot for YP4 in Fig. 4, with a clear contrast between the Neoproterozoic and Palaeoproterozoic age populations. Metamorphic apatites are commonly characterised by depletion of Th and LREE, particularly in metapelitic samples where the apatite coexists with monazite or epidote (Henrichs et al., 2018; Spear and Pyle, 2002). Figs. 6 and 8 show that apatites belonging to the Neoproterozoic age population in YP4 are enriched in LREE and have Th-U ratios >1:1. Based on these criteria, it seems unlikely that the younger apatite population is composed of apatites grown under metamorphic conditions.

The closure temperature of the U-Pb system in apatite is dependent on a number of factors, including the cooling rate, the size of the diffusion domain, and the presence of the conceptual "infinite reservoir" into which Pb can be lost (Blackburn et al., 2011). There is no systematic difference in the grain size or shape of apatites from each of the age populations in YP4, and given that these grains were separated from a quartzite it seems unlikely that they belonged to different chemical domains within the rock that may have inhibited diffusion of Pb (e. g. Blackburn et al., 2011) or were protected by grain armouring (e.g. Krenn and Finger, 2004). The greenschist facies metamorphism and corresponding temperatures experienced by the sample means that it is plausible that very slow cooling rates could induce resetting of the apatite U-Pb ages (Blackburn et al., 2011). However, the clear and well defined populations with no continuum of ages representing partially reset grains (Fig. 4) suggests that it is unlikely that the different age populations reflect resetting via thermally activated volume diffusion of radiogenic Pb. The distinct trace element and REE profiles that characterise each population further lends evidence to the argument that these are detrital populations. The closure temperatures of Sr and REEs in apatite are significantly higher than Pb (>550 °C; Cherniak, 2000), so it is unlikely that the observed geochemical differences between the populations reflect resetting via thermally activated volume diffusion under the temperature conditions this rock is thought to have experienced, suggesting a detrital origin for these geochemical populations.

In light of these consistent results from independent methods of classification, it seems most likely that the Neoproterozoic age apatite grains in YP4 were sourced from a Neoproterozoic magmatic rock of intermediate–mafic composition.

5.2.3. Above the Chingasan–Chapa unconformity

Apatites from three samples (YP15, 21, and 23) from above the Chingasan–Chapa unconformity were analysed, but only one (YP21) possesses zircon U-Pb data.

The sample from the lower part of the Nemchanka Formation of the Chapa Group, YP15, has two apatite age populations. An older, Palaeoproterozoic population contains ~26% of the grains, while the younger, rather scattered Neoproterozoic age population comprises the remaining ~74% of the grains.

Sample YP21, from the upper part of the Nemchanka Formation, records three peaks in both apatite and zircon data. Sample YP21 yielded 78 < 5% discordant zircon U-Pb ages that range from 834 ± 19 Ma to 2769 ± 15 Ma, with major peaks at ~1880 Ma and ~2580 Ma (Priyatkina et al., 2016). The YSG age is 834 ± 19 Ma. The youngest (Tonian) apatite age peak at 839 ± 39 Ma compares well with the zircon age peak at 834 ± 19 Ma (Priyatkina et al., 2016). The populations are similar in terms of age, but vary in the proportion of data that they represent. The youngest zircon population consists of only three grains, constituting only a very small proportion (4%) of the total zircon population, while this population in the apatite data contains 40% of all grains in the sample. This disparity may stem from biases in the generation or preservation of zircon relative to apatite. The large population of very old zircons is probably due to the persistence of these grains through several sedimentary, metamorphic or magmatic cycles, and does not accurately reflect the primary magmatic signature of the source (e. g. Andersen et al., 2016). The relative abundance of young apatites compared to zircon may suggest that a more mafic magmatic rock contributed significant amounts of sediment, or that a rock that experienced moderate–high grade metamorphism was a major source. The geochemical signatures for the apatite populations are similar to those for sample YP15 and are summarised below.

For the sample from the Cambrian Evenki Formation (YP23), only a single, highly scattered Neoproterozoic apatite age population was defined. The analyses are rather scattered in Tera-Wasserburg space, but have quite consistent REE profiles.

The Neoproterozoic age component of the Chapa Group and Evenki Formation rocks (above the unconformity) is significantly more abundant than the equivalent age population in the Chingasan and Sukhopit Group rocks (below the unconformity). Post-unconformity younger grains are relatively consistent between the samples in terms of REE characteristics, and notably different as a group from the young component below the Chingasan–Chapa unconformity (Fig. 9). These grains have mostly flat to LREE depleted REE profiles and strong negative Eu anomalies. This signature is characteristic of S-type and felsic I-type peraluminous granites (Sha and Chappell, 1999). The depletion of Th in most of these grains supports this interpretation as the expected crystallization of monazite prior to apatite in these rocks would also take up Th preferentially (Sha and Chappell, 1999).

The Palaeoproterozoic age component from the Chapa Group rocks is relatively small and does not have any strong defining characteristics. They tend to be flat to moderately enriched in LREE, have low Sr concentrations, low La/Nd ratios, and a range of Eu characteristics, from moderately negative to moderately positive anomalies, possibly indicating a felsic source (Figs. 5,7,8). In YP15 they tend to be enriched in Th, while in YP21 they are more often depleted in Th.

5.3. Sediment sources

The Palaeoproterozoic and Archaean age component throughout all the samples is derived from a mixture of sources, with no unifying geochemical characteristics within or between samples. This is expected, as this age component in the detrital zircon record is interpreted to represent material derived from the basement of the Siberian Craton (Priyatkina et al., 2016). In most samples, the population of zircons that records the oldest (>2000 Ma) ages represents a large proportion of all zircons, while in apatite these ages represent a much smaller proportion of the total population. This probably represents the decreased preservation potential of ancient apatite grains in terms of both chemical or mechanical destruction and U-Pb reset. These >2000 Ma grains in the apatite record do not form clear linear arrays in Tera-Wasserburg space and so the ages are poorly defined in addition to being relatively rare. The zircons of this age are interpreted in Priyatkina et al. (2016) to be derived from the granites and high-grade metamorphic rocks of the Tungus block (e.g. Rosen et al., 1994; Turkina et al., 2012).

The late Palaeoproterozoic age component at 2000–1750 Ma is characteristic of sediments derived from the Siberian Craton due to extensive magmatism at this time related to the amalgamation of Siberia (e. g. Gladkochub et al., 2013; Glorie et al., 2014; Powerman et al., 2015;

Safonova et al., 2010). This population is well defined in some apatite samples, although in other instances (e.g. YP6) it is difficult to distinguish between grains from an older source and the main (~1850 Ma) Palaeoproterozoic peak. The geochemical signatures of these grains are again quite mixed due to the range of sources, including a wide range of magmatism and high-grade metamorphic rocks of this age, that are common on the western margin of the Siberian Craton. The abundance of the 'Siberian' population changes throughout the stratigraphy. The relative increase in the numbers of older apatite grains from YP4 through YP8 up to YP6 is reversed across the Chingasan–Chapa unconformity, after which Palaeoproterozoic or older apatite are relatively rare. A more in-depth discussion of the provenance of the Archaean and Palaeoproterozoic zircons in these samples can be found in Priyatkina et al. (2016).

The source of the Neoproterozoic age component shows systematic changes throughout the stratigraphy (Fig. 9). There is a strong geochemical similarity between the Neoproterozoic age component of the deformed and metamorphosed rock from which YP4 was sampled and the unconformably overlying Chingasan rocks (YP6,8). The source of this population is most likely the mafic–intermediate volcanic equivalents of the Teya granite (880–860 Ma, Vernikovsky et al., 2007). In this interpretation, the early phases of the widespread 880–840 Ma magmatism in the Yenisey Ridge contribute material to the rock unit from which YP4 was sampled, which was subsequently deformed and metamorphosed.

The Chingasan Group rocks were then unconformably deposited onto the older metamorphosed rock. The samples from Chingasan rocks (YP6, 8) have a Neoproterozoic source similar to YP4, but the 'Siberian' age component is markedly different in terms of geochemistry. The Neoproterozoic component is also smaller in the Chingasan Group than in the older YP4, and decreases further in relative abundance in the upper part of the sequence (from YP8 to YP6), indicating the depletion of this source over time. The abundance of the Archaean component of the apatite and zircon populations also increases in the upper part of the Chingasan Group, suggesting an increase in sediment sourced from the Tungus block that is characterised by rocks of this age (e.g. Turkina et al., 2014).

The unconformity that demarcates the boundary between the Chingasan and Chapa Group rocks heralds a major change in the source and relative abundance of the Neoproterozoic age component. Apatites from the Chapa Group rocks are dominated by the Neoproterozoic age component, which has a geochemical signature that can be interpreted as deriving either from an evolved I or S type granite or from a metamorphic rock. Many of the intrusive igneous rocks in the Yenisey Ridge with ages of 880–840 Ma, such as the Teya, Kalami, and Yeruda plutons, are considered to be I to S type (e.g. Nozhkin et al., 2015; Vernikovsky et al., 2007). There are also abundant metamorphic rocks in the area, particularly the Teya Group, which experienced peak metamorphism at ~825 Ma (Likhanov et al., 2012). Thus, it is likely that the Chapa Group rocks were sourced mostly from the Yenisey Ridge, with perhaps some input from the Siberian Craton. This is consistent with palaeocurrent measurements from the Nemchanka Formation in the vicinity of YP21, indicating a NNE direction of flow from the core of the Yenisey Ridge outward onto the craton (Priyatkina et al., 2016).

6. Conclusion

In this study, we show how the analysis of detrital apatite can provide important and useful information about the source of sedimentary material, and how this information can be combined with zircon U-Pb data to take advantage of the complementary and intersecting archives of information these minerals contain. In particular, this approach can detect the presence of mafic source rocks that may go undetected through purely the use of detrital zircon analysis.

The trace element data presented in this study complement the apatite U-Pb data, providing information that explicitly ties the age of an apatite grain to the source rock. As such, this method is an improvement on approaches that rely on different materials to provide age (e.g. zircon U-Pb) and source rock information (e.g. whole rock geochemistry or heavy mineral analysis). When used in conjunction with detrital zircon analysis, the relative age abundance of detrital apatites can also provide further insight into the source of sediment and highlights biases in an interpretation based only on zircon U-Pb data.

The change in source detected in this study by the combination of apatite U-Pb and trace element analysis provides insight into the tectonic evolution of the region that could not be detected by either of these methods performed in isolation. We therefore recommend the use of multi-method apatite analysis as a new tool that can be applied to understand the source of sediment.

Acknowledgments

We thank C.L. Kirkland and an anonymous reviewer for providing helpful and constructive reviews, and the editor X-H. Li for handling the publication process swiftly and efficiently. This work was financially supported by an Australian Research Council Discovery Project (DP150101730). JG is supported by an Australian Government Research Training Program Scholarship. Sarah Gilbert and Adelaide Microscopy are thanked for support and guidance with analytical procedure. Samples were provided by N·Priyatkina. Comments by A.Nozhkin and E. Letnikova were helpful for understanding of local geology. Study of A. Khudoley was supported by St. Petersburg State University research grant # 3.38.137.2014. This paper forms TRaX record #399.

Appendix A. Supplementary data

Supplementary data to this article can be found online at https://doi.org/10.1016/j.lithos.2018.05.026.

References

Abdullin, F., Solé, J., Solari, L., Shchepetilnikova, V., Meneses-Rocha, J.J., Pavlinova, N., Rodríguez-Trejo, A., 2016. Single-grain apatite geochemistry of Permian–Triassic granitoids and Mesozoic and Eocene sandstones from Chiapas, Southeast Mexico: implications for sediment provenance. Int. Geol. Rev. 58, 1132–1157.

Andersen, T., Kristoffersen, M., Elburg, M.A., 2016. How far can we trust provenance and crustal evolution information from detrital zircons? A south African case study. Gondwana Res. 34, 129–148.

Armistead, S.E., Collins, A.S., Payne, J.L., Foden, J.D., De Waele, B., Shaji, E., Santosh, M., 2018. A re-evaluation of the Kumta suture in western peninsular India and its extension into Madagascar. J. Asian Earth Sci. 157, 317–328.

Belousova, E.A., Griffin, W.L., O'Reilly, S.Y., Fisher, N.I., 2002. Apatite as an indicator mineral for mineral exploration: trace-element compositions and their relationship to host rock type. J. Geochem. Explor. 76, 45–69.

Blackburn, T., Bowring, S.A., Schoene, B., Mahan, K., Dudas, F., 2011. U-Pb thermochronology: creating a temporal record of lithosphere thermal evolution. Contrib. Mineral. Petrol. 162, 479–500.

Bruand, E., Storey, C., Fowler, M., 2016. An apatite for progress: inclusions in zircon and titanite constrain petrogenesis and provenance. Geology 44, 91–94.

Bruand, E., Fowler, M., Storey, C., Darling, J., 2017. Apatite trace element and isotope applications to petrogenesis and provenance. Am. Mineral. 75.

Bruguier, O., Lancelot, J.R., Malavieille, J., 1997. U–Pb dating on single detrital zircon grains from the Triassic Songpan–Ganze flysch (Central China): provenance and tectonic correlations. Earth Planet. Sci. Lett. 152, 217–231.

Carrapa, B., DeCelles, P.G., Reiners, P.W., Gehrels, G.E., Sudo, M., 2009. Apatite triple dating and white mica 40Ar/39Ar thermochronology of syntectonic detritus in the Central Andes: a multiphase tectonothermal history. Geology 37, 407–410.

Cawood, P.A., Nemchin, A.A., Freeman, M., Sircombe, K., 2003. Linking source and sedimentary basin: detrital zircon record of sediment flux along a modern river system and implications for provenance studies. Earth Planet. Sci. Lett. 210, 259–268.

Cherniak, D.J., 2000. Rare earth element diffusion in apatite. Geochim. Cosmochim. Acta 64, 3871–3885.

Chew, D.M., Donelick, R.A., Donelick, M.B., Kamber, B.S., Stock, M.J., 2014a. Apatite chlorine concentration measurements by LA-ICP-MS. Geostand. Geoanal. Res. 38, 23–35.

Chew, D.M., Petrus, J.A., Kamber, B.S., 2014b. U–Pb LA–ICPMS dating using accessory mineral standards with variable common Pb. Chem. Geol. 363, 185–199.

Chew, D.M., Babechuk, M.G., Cogné, N., Mark, C., O'Sullivan, G.J., Henrichs, I.A., Doepke, D., McKenna, C.A., 2016. (LA,Q)-ICPMS trace-element analyses of Durango and McClure Mountain apatite and implications for making natural LA-ICPMS mineral standards. Chem. Geol. 435, 35–48.

Chu, M.-F., Wang, K.-L., Griffin, W.L., Chung, S.-L., O'Reilly, S.Y., Pearson, N.J., Iizuka, Y., 2009. Apatite composition: tracing petrogenetic processes in Transhimalayan Granitoids. J. Petrol. 50, 1829–1855.
Cochrane, R., Spikings, R.A., Chew, D., Wotzlaw, J.-F., Chiaradia, M., Tyrrell, S., Schaltegger, U., Van der Lelij, R., 2014. High temperature (>350°C) thermochronology and mechanisms of Pb loss in apatite. Geochim. Cosmochim. Acta 127, 39–56.
Dickinson, W.R., 2008. Impact of differential zircon fertility of granitoid basement rocks in North America on age populations of detrital zircons and implications for granite petrogenesis. Earth Planet. Sci. Lett. 275, 80–92.
Dickinson, W.R., Gehrels, G.E., 2003. U–Pb ages of detrital zircons from Permian and Jurassic eolian sandstones of the Colorado plateau, USA: paleogeographic implications. Sediment. Geol. 163, 29–66.
Dill, H.G., 1994. Can REE patterns and U-Th variations be used as a tool to determine the origin of apatite in clastic rocks? Sediment. Geol. 92, 175–196.
Fleischer, M., Altschuler, Z.S., 1986. The lanthanides and yttrium in minerals of the apatite group - an analysis of the available data. Neues Jahrbuch fuer Mineralogie, Monatshefte 10, 467–480.
Gibson, G.M., Ireland, T.R., 1996. Extension of Delamerian (Ross) orogen into western New Zealand: evidence from zircon ages and implications for crustal growth along the Pacific margin of Gondwana. Geology 24, 1087–1090.
Gladkochub, D.P., Stanevich, A.M., Mazukabzov, A.M., Donskaya, T.V., Pisarevsky, S.A., Nicoll, G., Motova, Z.L., Kornilova, T.A., 2013. Early evolution of the Paleoasian Ocean: LA-ICP-MS dating of detrital zircon from Late Precambrian sequences of the southern margin of the Siberian craton. Russ. Geol. Geophys. 54, 1150–1163.
Glorie, S., De Grave, J., Buslov, M.M., Zhimulev, F.I., Safonova, I.Y., 2014. Detrital zircon provenance of early Palaeozoic sediments at the southwestern margin of the Siberian Craton: insights from U–Pb geochronology. J. Asian Earth Sci. 82, 115–123.
Henrichs, I.A., O'Sullivan, G., Chew, D.M., Mark, C., Babechuk, M.G., McKenna, C., Emo, R., 2018. The trace element and U-Pb systematics of metamorphic apatite. Chem. Geol. 483, 218–238.
Hinton, R.W., 1999. NIST SRM 610, 611 and SRM 612, 613 multi-element glasses: constraints from element abundance ratios measured by microprobe techniques. Geostand. Newslett. 23, 197–207.
Jafarzadeh, M., Harami, R.M., Friis, H., Amini, A., Mahboubi, A., Lenaz, D., 2014. Provenance of the Oligocene–Miocene Zivah formation, NW Iran, assessed using heavy mineral assemblage and detrital clinopyroxene and detrital apatite analyses. J. Afr. Earth Sci. 89, 56–71.
Jennings, E.S., Marschall, H.R., Hawkesworth, C.J., Storey, C.D., 2011. Characterization of magma from inclusions in zircon: apatite and biotite work well, feldspar less so. Geology 39, 863–866.
Jepson, G., Glorie, S., Konopelko, D., Gillespie, J., Danišík, M., Evans, N.J., Mamadjanov, Y., Collins, A.S., 2018. Thermochronological insights into the structural contact between the Tian Shan and Pamirs, Tajikistan. Terra Nova 30, 95–104.
Krenn, E., Finger, F., 2004. Metamorphic formation of Sr-apatite and Sr-bearing monazite in a high-pressure rock from the Bohemian Massif. Am. Mineral. 89, 1323–1329.
Kuzmichev, A.B., Sklyarov, E.V., 2016. The Precambrian of Transangaria, Yenisei Ridge (Siberia): Neoproterozoic microcontinent, Grenville-age orogen, or reworked margin of the Siberian craton? J. Asian Earth Sci. 115, 419–441.
LaMaskin, T.A., 2012. Detrital zircon facies of Cordilleran terranes in western North America. GSA Today 22, 4–11.
Likhanov, I.I., Reverdatto, V.V., 2007. Provenance of Precambrian Fe- and Al-rich Metapelites in the Yenisey Ridge and Kuznetsk Alatau, Siberia: geochemical signatures. Acta Geol. Sin. Eng. Ed. 81, 409–423.
Likhanov, I.I., Santosh, M., 2017. Neoproterozoic intraplate magmatism along the western margin of the Siberian Craton: implications for breakup of the Rodinia supercontinent. Precambrian Res. 300, 315–331.
Likhanov, I.I., Kozlov, P.S., Polyansky, O.P., Popov, N.V., Reverdatto, V.V., Travin, A.V., Vershinin, A.E., 2007. Neoproterozoic age of collisional metamorphism in the Transangara region of the Yenisei Ridge (based on 40Ar/39Ar data). Dokl. Earth Sci. 413, 234–237.
Likhanov, I.I., Reverdatto, V.V., Vershinin, A.E., 2008. Fe- and Al-rich metapelites of the Teiskaya Group, Yenisei Range: geochemistry, protoliths, and the behavior of their material during metamorphism. Geochem. Int. 46, 17–36.
Likhanov, I.I., Reverdatto, V.V., Kozlov, P.S., 2012. U-Pb and 40Ar/39Ar evidence for Grenvillian activity in the Yenisey Ridge during formation of the Teya metamorphic complex. Geochem. Int. 50, 551–557.
Likhanov, I.I., Nozhkin, A.D., Reverdatto, V.V., Kozlov, P.S., 2014. Grenville tectonic events and evolution of the Yenisei Ridge at the western margin of the Siberian Craton. Geotectonics 48, 371–389.
Likhanov, I.I., Reverdatto, V.V., Kozlov, P.S., Khiller, V.V., Sukhorukov, V.P., 2015. P-T-t constraints on polymetamorphic complexes of the Yenisey Ridge, East Siberia: implications for Neoproterozoic paleocontinental reconstructions. J. Asian Earth Sci. 113, 391–410.
Malusà, M.G., Resentini, A., Garzanti, E., 2016. Hydraulic sorting and mineral fertility bias in detrital geochronology. Gondwana Res. 31, 1–19.
Mark, C., Cogné, N., Chew, D., 2016. Tracking exhumation and drainage divide migration of the Western Alps: a test of the apatite U-Pb thermochronometer as a detrital provenance tool. Geol. Soc. Am. Bull. 128, 1439–1460.
McDowell, F.W., McIntosh, W.C., Farley, K.A., 2005. A precise 40Ar–39Ar reference age for the Durango apatite (U–Th)/He and fission-track dating standard. Chem. Geol. 214, 249–263.
Mel'nikov, N.V., Yakshin, M.S., Shishkin, B.B., Efimov, A.O., Karlova, G.A., Kilina, L.I., Konstantinova, L.N., Kochnev, B.B., Kraevsky, B.G., Mel'nikov, P.N., Nagovitsin, K.E., Postnikov, A.A., Ryabkova, L.V., Terleev, A.A., Khabarov, E.M., 2005. The Riphean and Vendian Strata of the Siberian Platform and its folded framing [in Russian]. In: Mel'nikov, N.V. (Ed.), Stratigraphy of Petroliferous Basins of Siberia. Academic Publishing House "Geo, Novosibirsk, p. 428.
Merdith, A.S., Collins, A.S., Williams, S.E., Pisarevsky, S., Foden, J.D., Archibald, D.B., Blades, M.L., Alessio, B.L., Armistead, S., Plavsa, D., Clark, C., Müller, R.D., 2017. A full-plate global reconstruction of the Neoproterozoic. Gondwana Res. 50, 84–134.
Moecher, D.P., Samson, S.D., 2006. Differential zircon fertility of source terranes and natural bias in the detrital zircon record: implications for sedimentary provenance analysis. Earth Planet. Sci. Lett. 247, 252–266.
Morton, A.C., Hallsworth, C.R., 1999. Processes controlling the composition of heavy mineral assemblages in sandstones. Sediment. Geol. 124, 3–29.
Morton, A., Yaxley, G., 2007. Detrital apatite geochemistry and its application in provenance studies. Geol. Soc. Am. Spec. Pap. 420, 319–344.
Nozhkin, A.D., Postnikov, A.A., Nagovitsin, K.E., Travin, A.V., Stanevich, A.M., Yudin, D.S., 2007. Neoproterozoic Chingasan Group in the Yenisei Ridge: new data on age and deposition environments. Russ. Geol. Geophys. 48, 1015–1025.
Nozhkin, A.D., Turkina, O.M., Maslov, A.V., Dmitrieva, N.V., Kovach, V.P., Ronkin, Y.L., 2008. Sm-Nd isotopic systematics of precambrian metapelites from the Yenisei range and age variations of their provenances. Dokl. Earth Sci. 423, 1495–1500.
Nozhkin, A.D., Maslov, A.V., Podkovyrov, V.N., Turkina, O.M., Letnikova, E.F., Ronkin, Y.L., Krupenin, M.T., Dmitrieva, N.V., Gareev, E.Z., Lepikhina, O.P., 2009. Geochemistry of Riphean terrigenous rocks in the southern Urals and Siberia and variations of the continental-crust maturity. Russ. Geol. Geophys. 50, 71–86.
Nozhkin, A.D., Borisenko, A.S., Nevol'ko, P.A., 2011. Stages of Late Proterozoic magmatism and periods of Au mineralization in the Yenisei Ridge. Russ. Geol. Geophys. 52, 124–143.
Nozhkin, A.D., Maslov, A.V., Dmitrieva, N.V., Ronkin, Y.L., 2012. Pre-Riphean metapelites of the Yenisei Range: chemical composition, sources of eroded material, and paleogeodynamics. Geochem. Int. 50, 574–610.
Nozhkin, A.D., Popov, N.V., Dmitrieva, N.V., Storozhenko, A.A., Vasil'ev, N.F., 2015. Neoproterozoic collisional S-type granitoids of the Yenisei Ridge: petrogeochemical composition and U-Pb, Ar-Ar, and Sm-Nd isotope data. Russ. Geol. Geophys. 56, 689–695.
Oksanen, J., Blanchet, F.G., Friendly, M., Kindt, R., Legendre, P., McGlinn, D., Minchin, P.R., O'Hara, R.B., Simpson, G.L., Solymos, P., Stevens, M.H.H., Szoecs, E., Wagner, H., 2017. Vegan: Community Ecology Package.
Painter, C.S., Carrapa, B., DeCelles, P.G., Gehrels, G.E., Thomson, S.N., 2014. Exhumation of the North American Cordillera revealed by multi-dating of Upper Jurassic–Upper Cretaceous foreland basin deposits. Geol. Soc. Am. Bull. 126, 1439–1464.
Paton, C., Hellstrom, J., Paul, B., Woodhead, J., Hergt, J., 2011. Iolite: freeware for the visualisation and processing of mass spectrometric data. J. Anal. At. Spectrom. 26, 2508–2518.
Piccoli, P.M., Candela, P.A., 2002. Apatite in igneous systems. Rev. Mineral. Geochem. 48, 255–292.
Pokrovsky, B.G., Bujakaite, M.I., Kokin, O.V., 2012. Geochemistry of C, O, and Sr isotopes and chemostratigraphy of neoproterozoic rocks in the northern Yenisei ridge. Lithol. Miner. Resour. 47, 177–199.
Powerman, V., Shatsillo, A., Chumakov, N., Kapitonov, I., Hourigan, J., 2015. Interaction between the Central Asian Orogenic Belt (CAOB) and the Siberian craton as recorded by detrital zircon suites from Transbaikalia. Precambrian Res. 267, 39–71.
Priyatkina, N., Khudoley, A.K., Collins, W.J., Kuznetsov, N.B., Huang, H.-Q., 2016. Detrital zircon record of Meso- and Neoproterozoic sedimentary basins in northern part of the Siberian Craton: characterizing buried crust of the basement. Precambrian Res. 285, 21–38.
Rosen, O.M., Condie, K.C., Natapov, L.M., Nozhkin, A.D., 1994. Chapter 10 Archean and Early Proterozoic evolution of the Siberian Craton: a preliminary assessment. In: Condie, K.C. (Ed.), Developments in Precambrian Geology. Elsevier, pp. 411–459.
Safonova, I., Maruyama, S., Hirata, T., Kon, Y., Rino, S., 2010. LA ICP MS U–Pb ages of detrital zircons from Russia largest rivers: implications for major granitoid events in Eurasia and global episodes of supercontinent formation. J. Geodyn. 50, 134–153.
Schoene, B., 2014. 4.10 - U–Th–Pb Geochronology A2 - Holland, Heinrich D. In: Turekian, K.K. (Ed.), Treatise on Geochemistry, Second Edition Elsevier, Oxford, pp. 341–378.
Schoene, B., Bowring, S.A., 2006. U–Pb systematics of the McClure Mountain syenite: thermochronological constraints on the age of the 40Ar/39Ar standard MMhb. Contrib. Mineral. Petrol. 151, 615.
Schoene, B., Bowring, S.A., 2007. Determining accurate temperature–time paths from U–Pb thermochronology: an example from the Kaapvaal craton, southern Africa. Geochim. Cosmochim. Acta 71, 165–185.
Sha, L.-K., Chappell, B.W., 1999. Apatite chemical composition, determined by electron microprobe and laser-ablation inductively coupled plasma mass spectrometry, as a probe into granite petrogenesis. Geochim. Cosmochim. Acta 63, 3861–3881.
Spear, F.S., Pyle, J.M., 2002. Apatite, monazite, and xenotime in metamorphic rocks. Rev. Mineral. Geochem. 48, 293–335.
Spencer, C.J., Kirkland, C.L., Roberts, N.M.W., 2018. Implications of erosion and bedrock composition on zircon fertility; examples from South America and Western Australia. Terra Nova 1–7.
Stacey, J.S., Kramers, J.D., 1975. Approximation of terrestrial lead isotope evolution by a two-stage model. Earth Planet. Sci. Lett. 26, 207–221.
Sun, S.-s., McDonough, W.F., 1989. Chemical and isotopic systematics of oceanic basalts: implications for mantle composition and processes. Geol. Soc. Lond., Spec. Publ. 42, 313–345.
Thomson, S.N., Gehrels, G.E., Ruiz, J., Buchwaldt, R., 2012. Routine low-damage apatite U-Pb dating using laser ablation–multicollector–ICPMS. Geochem. Geophys. Geosyst. 13, n/a.
Turkina, O.M., Berezhnaya, N.G., Lepekhina, E.N., Kapitonov, I.N., 2012. U–Pb (SHRIMP II), Lu–Hf isotope and trace element geochemistry of zircons from high-grade metamorphic rocks of the Irkut terrane, Sharyzhalgay uplift: implications for the Neoarchaean evolution of the Siberian Craton. Gondwana Res. 21, 801–817.
Turkina, O.M., Lepekhina, E.N., Berezhnaya, N.G., Kapitonov, I.N., 2014. U-Pb age and Lu-Hf isotope systematics of detrital zircons from paragneiss of the Bulun block

(Sharyzhalgai uplift of the Siberian Craton Basement). Dokl. Earth Sci. 458, 1265–1272.

Varganov, A.S., Moskalev, V.A., Barmin, V.A., 2010. Sheet P-46 (North Yeniseysk), Geological State Map of the Russian Federation, scale 1:1000000. VSEGEI Press, St. Petersburg.

Vermeesch, P., 2012. On the visualisation of detrital age distributions. Chem. Geol. 312–313, 190–194.

Vermeesch, P., 2013. Multi-sample comparison of detrital age distributions. Chem. Geol. 341, 140–146.

Vernikovsky, V.A., Vernikovskaya, A.E., Kotov, A.B., Sal'nikova, E.B., Kovach, V.P., 2003. Neoproterozoic accretionary and collisional events on the western margin of the Siberian craton: new geological and geochronological evidence from the Yenisey Ridge. Tectonophysics 375, 147–168.

Vernikovsky, V.A., Vernikovskaya, A.E., Wingate, M.T.D., Popov, N.V., Kovach, V.P., 2007. The 880–864Ma granites of the Yenisey Ridge, western Siberian margin: geochemistry, SHRIMP geochronology, and tectonic implications. Precambrian Res. 154, 175–191.

Vernikovsky, V.A., Metelkin, D.V., Vernikovskaya, A.E., Matushkin, N.Y., Kazansky, A.Y., Kadilnikov, P.I., Romanova, I.V., Wingate, M.T.D., Larionov, A.N., Rodionov, N.V., 2016. Neoproterozoic tectonic structure of the Yenisei Ridge and formation of the western margin of the Siberian craton based on new geological, paleomagnetic, and geochronological data. Russ. Geol. Geophys. 57, 47–68.

Volobuev, M.I., Zykov, S.I., Stupnikova, N.I., Strizhov, V.P., Myasnikova, V.L., 1976. Age of the basement and geosynclinal formations of the grenvillides in the Yenisei Range (in Russian). Determination of the Isotopic Age of Ore Deposits, pp. 39–47.

Yang, B., Smith, T.M., Collins, A.S., Munson, T.J., Schoemaker, B., Nicholls, D., Cox, G., Farkas, J., Glorie, S., 2018. Spatial and temporal variation in detrital zircon age provenance of the hydrocarbon-bearing upper Roper Group, Beetaloo Sub-basin, Northern Territory, Australia. Precambrian Res. 304, 140–155.

Zattin, M., Andreucci, B., Thomson, S.N., Reiners, P.W., Talarico, F.M., 2012. New constraints on the provenance of the ANDRILL AND-2A succession (western Ross Sea, Antarctica) from apatite triple dating. Geochem. Geophys. Geosyst. 13 (n/a-n/a).